J. Fluid Mech. (2003), *vol.* 477, *pp.* 227–257. © 2003 Cambridge University Press
DOI: 10.1017/S0022112002003002 Printed in the United Kingdom

The nonlinear instability of thread–annular flow at high Reynolds number

By ANDREW G. WALTON

Mathematics Department, Imperial College of Science, Technology & Medicine, 180 Queen's Gate, London SW7 2BZ, UK

(Received 18 June 2002 and in revised form 14 September 2002)

The surgical technique of thread injection of medical implants is modelled by the axial pressure-gradient-driven flow between concentric cylinders with a moving core. The nonlinear stability of the basic flow is analysed theoretically at asymptotically large Reynolds number and it is found that non-axisymmetric finite-amplitude neutral modes can be supported over a wide range of thread radii and injection velocities. The axial force on the thread is calculated and it is found to be significantly less than that predicted by undisturbed-flow theory, in agreement with thread–annular experiments.

1. Introduction

Thread injection is a newly devised surgical technique which enables porous medical implants to be placed inside the body in a minimally invasive way, thus reducing surgical trauma. The thread is stored on a spool and injected within a fluid by applying an axial pressure gradient to the cylindrical container holding the liquid and the thread (figure 1). The thread velocity V^* is controlled by a motor. It is clearly desirable for the thread to be injected smoothly and to not suffer lateral deviation: it is therefore important that the flow is kept laminar. For this reason the transition to turbulence of the basic thread–annular flow and its dependence upon Reynolds number, thread radius and injection velocity are of great practical interest.

In a recent experimental paper Frei, Lüscher & Wintermantel (2000, hereinafter referred to as FLW) modelled the thread injection process by using a cylindrical rubber filament to represent the thread. The filament was allowed to move concentrically through a steel cylindrical pipe (representing the injection vessel) filled with water. They measured various quantities including the axial force on the thread due to pressure gradient and viscous effects. On comparing the results with the theoretical predictions that arise from the exact Navier–Stokes solution for axial flow between concentric cylinders they discovered that the force measured in the experiments was always significantly less than that predicted by their theory. This observation forms the motivation for the current study in which we investigate whether this discrepancy could be caused by a nonlinear instability of the basic thread–annular flow.

There have been many theoretical studies of the stability of so-called core–annular flows in which two fluids with different properties occupy a single pipe (e.g. the temporal studies of Preziosi, Chen & Joseph 1989 and Huang & Joseph 1995 and the spatio-temporal approach of Shen & Li 1996 and Chen & Lin 2002). In recent years there has been less attention focused on the case where the inner cylinder is a solid body rather than a fluid. The exact solution of the Navier–Stokes equations

https://doi.org/10.1017/S0022112002003002 Published online by Cambridge University Press

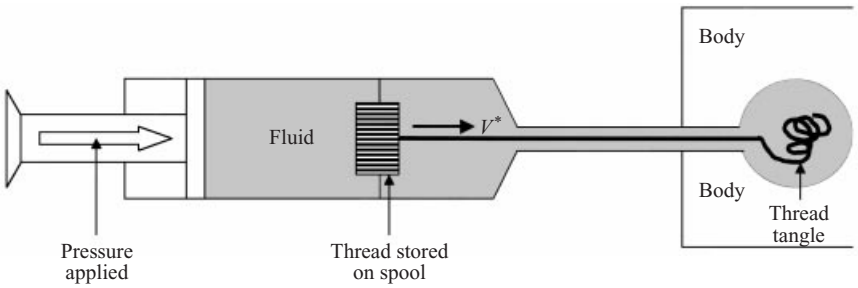


FIGURE 1. The thread injection process: fluid is forced out of the container and along the pipe; simultaneously, the thread is injected using a motor attached to the spool. The thread forms a porous tangle in the desired location within the body.

that arises in this case (to be derived in § 1.1) was studied by Shigechi & Lee (1991) and is also used by FLW, but although the linear stability of this flow has been discussed extensively by Mott & Joseph (1968) and Sadeghi & Higgins (1991) the critical Reynolds number predictions from these studies are much higher than those observed experimentally. It would therefore appear that nonlinear effects are particularly important at an early stage in the transition process for this flow.

The stability approach adopted in this paper is to study the thread–annular flow at high Reynolds number and seek a nonlinear neutral wave instability structure in which the critical layer (where the disturbance phase speed matches that of the basic flow) is sited away from the annulus walls and is of the nonlinear inviscid type first studied by Benney & Bergeron (1969). We find that the nonlinear disturbances have a particularly strong effect on the mean flow. The stability structure found here is similar to that derived by Smith & Bodonyi (1982) for flow through a circular pipe, but there are a number of crucial differences which will be highlighted in § 2. Before moving on to discuss the instability in more detail we introduce the governing non-dimensional equations and derive the basic thread–annular flow.

1.1. *The governing equations and basic flow*

The cylindrical polar coordinate system $(x^*, r^*, \theta) = (a^* x, a^* r, \theta)$ is used throughout this paper, where x, r and θ represent the non-dimensional axial, radial and azimuthal coordinates respectively and the tube is of dimensional radius a^*. The velocity components are written as $(u^*, v^*, w^*) = (g^* a^{*2}/\rho^* \nu^*)(u, v, w)$, where $-4g^*$ is the constant axial pressure gradient to be applied to the pipe. Here ρ^* and ν^* are the density and kinematic viscosity of the incompressible fluid. We express the pressure p^* as $(g^{*2} a^{*4}/\rho^* \nu^{*2})p$, and the time is written in the form $(\rho^* \nu^*/g^* a^*)t$. These scalings enable us to write the governing three-dimensional, unsteady Navier–Stokes equations in the non-dimensional form:

$$\frac{\partial u}{\partial x} + \frac{\partial v}{\partial r} + \frac{v}{r} + \frac{1}{r}\frac{\partial w}{\partial \theta} = 0, \tag{1.1a}$$

$$\frac{\partial u}{\partial t} + u\frac{\partial u}{\partial x} + v\frac{\partial u}{\partial r} + \frac{w}{r}\frac{\partial u}{\partial \theta} = -\frac{\partial p}{\partial x} + \frac{1}{R}\left(\frac{\partial^2 u}{\partial x^2} + \frac{\partial^2 u}{\partial r^2} + \frac{1}{r}\frac{\partial u}{\partial r} + \frac{1}{r^2}\frac{\partial^2 u}{\partial \theta^2}\right), \tag{1.1b}$$

$$\frac{\partial v}{\partial t} + u\frac{\partial v}{\partial x} + v\frac{\partial v}{\partial r} + \frac{w}{r}\frac{\partial v}{\partial \theta} - \frac{w^2}{r} = -\frac{\partial p}{\partial r} + \frac{1}{R}\left(\frac{\partial^2 v}{\partial x^2} + \frac{\partial^2 v}{\partial r^2} + \frac{1}{r}\frac{\partial v}{\partial r} + \frac{1}{r^2}\frac{\partial^2 v}{\partial \theta^2} - \frac{v}{r^2} - \frac{2}{r^2}\frac{\partial w}{\partial \theta}\right), \tag{1.1c}$$

https://doi.org/10.1017/S0022112002003002 Published online by Cambridge University Press

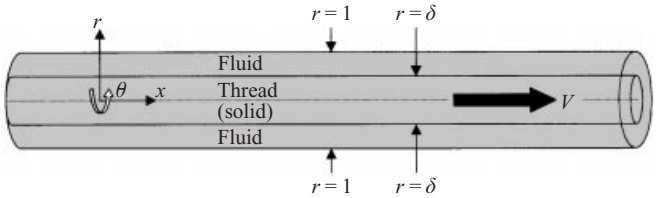


FIGURE 2. The simplified model geometry for which the Navier–Stokes equations have as a solution the basic thread–annular flow derived in § 1.

$$\frac{\partial w}{\partial t}+u\frac{\partial w}{\partial x}+v\frac{\partial w}{\partial r}+\frac{w}{r}\frac{\partial w}{\partial \theta}+\frac{vw}{r}$$
$$=-\frac{1}{r}\frac{\partial p}{\partial \theta}+\frac{1}{R}\left(\frac{\partial^2 w}{\partial x^2}+\frac{\partial^2 w}{\partial r^2}+\frac{1}{r}\frac{\partial w}{\partial r}+\frac{1}{r^2}\frac{\partial^2 w}{\partial \theta^2}-\frac{w}{r^2}+\frac{2}{r^2}\frac{\partial v}{\partial \theta}\right), \quad (1.1d)$$

where the Reynolds number R is defined by

$$R=\frac{g^* a^{*3}}{\rho^* v^{*2}}. \quad (1.2)$$

We wish to model the thread injection process by considering the axial flow between concentric cylinders $r = 1$ (representing the tube) and $r = \delta$ (representing a thread of dimensional radius $\delta^* = a^*\delta$). The thread is moving in the axial direction with non-dimensional velocity V (corresponding to the dimensional velocity $V^* = (g^* a^{*2}/\rho^* v^*)V = (v^*/a^*)RV$, from (1.2)). Figure 2 shows the geometrical configuration under consideration. The basic flow is expected to be steady and parallel so we seek a solution of the Navier–Stokes equations (1.1) in which

$$u = U_0(r), \qquad v = w = 0,$$

subject to the fixed axial pressure gradient $\partial p^*/\partial x^* = -4g^*$, which in non-dimensional terms can be written

$$\frac{\partial p}{\partial x}=-\frac{4}{R}.$$

From substitution into (1.1) the governing equation for U_0 is

$$U_0''+\frac{1}{r}U_0'=-4,$$

subject to the viscous no-slip conditions

$$U_0(\delta)=V, \qquad U_0(1)=0.$$

The solution is easily found to be

$$U_0=1-r^2+\frac{(V-1+\delta^2)}{\ln\delta}\ln r, \qquad \delta\leqslant r\leqslant 1. \quad (1.3)$$

Clearly this basic flow depends on two parameters: the thread radius δ, which must lie in the range $0<\delta<1$, and the thread injection velocity V. There is a theoretical maximum thread velocity at which the negative viscous shear force on the thread is balanced by that due to the pressure gradient. It will be shown in § 5 that this is given by

$$V_{\max}=1-\delta^2. \quad (1.4)$$

In figure 3 we plot the basic flow for various values of δ and V within their allowable

https://doi.org/10.1017/S0022112002003002 Published online by Cambridge University Press

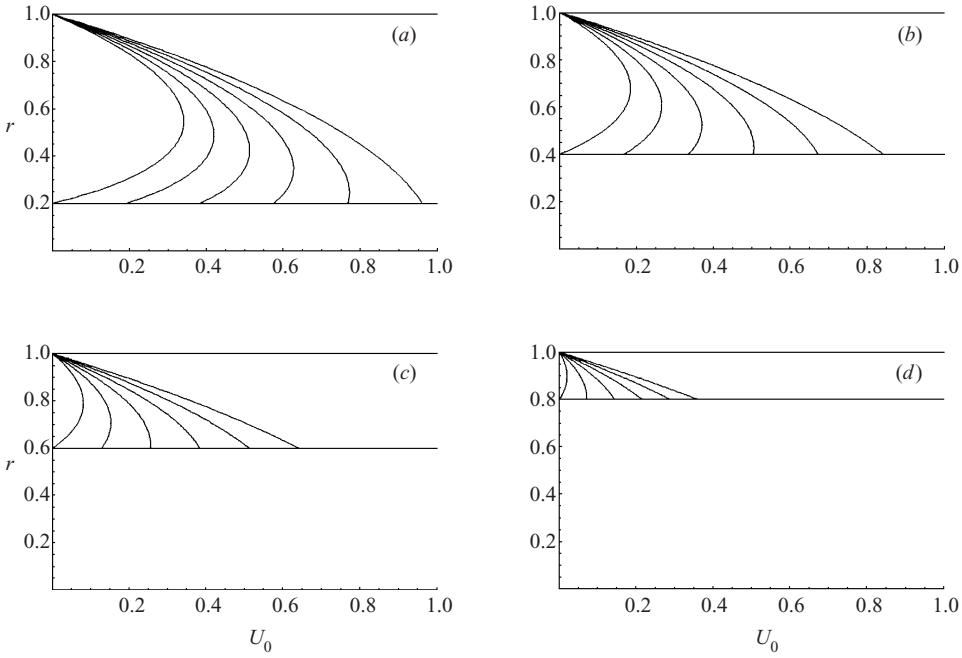


FIGURE 3. The basic thread–annular flow $U_0(r)$ for various values of thread radius δ and injection velocity V. (*a*) $\delta = 0.2$; (*b*) $\delta = 0.4$; (*c*) $\delta = 0.6$; (*d*) $\delta = 0.8$. In each case six equally spaced values of V are shown, ranging from (left to right) $V = 0$ to $V = V_{\max} = 1 - \delta^2$.

range. Since the pressure gradient rather than the mass flux is kept fixed we see that the mean velocity decreases as the thread radius is increased.

As remarked earlier there is a notable discrepancy between the results of thread-injection experiments and theory assuming the basic profile U_0. For example, Koch & Feind (1958) report that the experimental transitional Reynolds number R_c for thread–annular flow with a stationary thread lies in the range 3000–4000. On the other hand, linear theory (Sadeghi & Higgins 1991) only agrees well with experiment in the small-gap limit and generally predicts much higher values of R_c, with $R_c \to \infty$ as $\delta \to 0$ for all values of V. In this paper we will attempt to show that a possible reason for this discrepancy is that the basic flow is susceptible to a nonlinear instability which induces a distortion to the mean flow. To this end, in the next section we investigate the stability of the basic thread–annular flow to nonlinear non-axisymmetric disturbances using asymptotic methods based on a large-Reynolds-number assumption.

2. The nonlinear instability structure

In this section we will show that the basic thread–annular flow derived in § 1.1 supports a nonlinear neutral wave structure of a similar type to that found by Smith & Bodonyi (1982) for fully developed flow through a single pipe (Hagen–Poiseuille flow or HPF) and that found by Walton (2002) for impulsively started pipe flow. The neutral wave structure essentially consists of four main regions: a region where to leading order the instability is governed by inviscid dynamics; two viscous wall layers on the inner surface of the tube and the surface of the thread, and finally, and most significantly, an inviscid nonlinear equilibrium critical layer where the basic flow velocity is equal to the phase speed of the disturbance. The phase shifts induced

https://doi.org/10.1017/S0022112002003002 Published online by Cambridge University Press

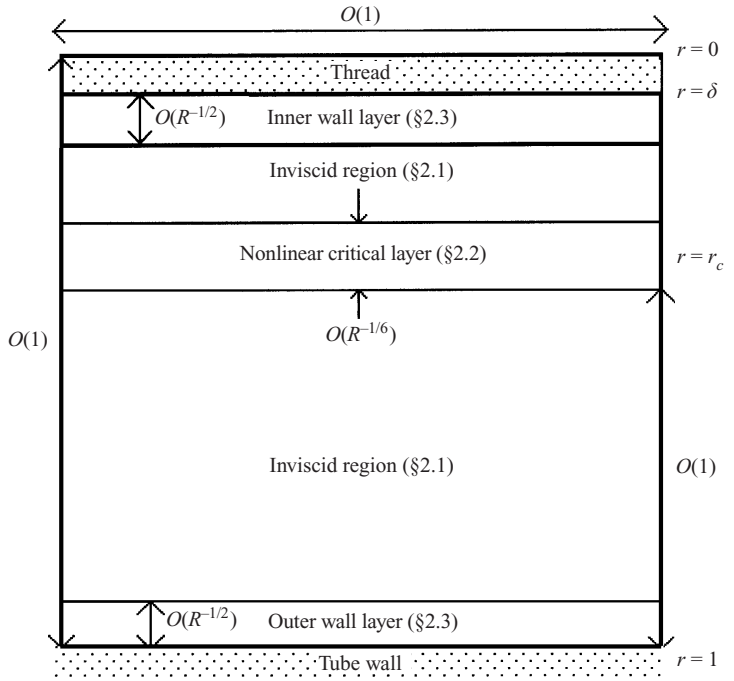


FIGURE 4. The asymptotic structure of the nonlinear neutral modes for thread–annular flow.

across the two wall layers must be balanced by that induced across the critical layer and this requirement leads to the determination of the amplitude of the disturbance in terms of its azimuthal and axial wavenumbers and the properties of the basic flow. A sketch of the neutral wave structure is given in figure 4. We start by considering the inviscid part of the flow field before embarking upon the more complicated critical layer analysis.

2.1. *The inviscid region*

This region occupies the majority of the pipe where the radial variable r is $O(1)$. The scalings follow those set out in Smith & Bodonyi (1982, hereinafter referred to as SB) and the appropriate expansions are:

$$u = U_0(r) + R^{-1/6}u_{1M}(r) + R^{-1/3}(u_2(r,\theta,x) + u_{2M}(r)) + \cdots + R^{-5/6}u_5(r,\theta,x) + \cdots, \quad (2.1a)$$

$$v = R^{-1/3}v_2(r,\theta,x) + \cdots + R^{-5/6}v_5(r,\theta,x) + \cdots, \quad (2.1b)$$

$$w = R^{-1/6}w_{1M}(r) + R^{-1/3}(w_2(r,\theta,x) + w_{2M}(r)) + \cdots + R^{-5/6}w_5(r,\theta,x) + \cdots, \quad (2.1c)$$

$$p = R^{-1/3}(p_2(r,\theta,x) + p_{2M}(r)) + \cdots + R^{-5/6}p_5(r,\theta,x) + \cdots, \quad (2.1d)$$

with $R \gg 1$. The subscript M refers to a mean flow distortion which is the subject of a detailed discussion in §4, but it is worth noting at this stage that the induced streamwise and azimuthal mean-flow distortions are larger than the fundamental disturbance, which has the subscript 2. The appearance of the terms with subscript 5 anticipate the occurrence of the induced $O(R^{-1/2})$ phase shift to be discussed in more detail in §2.2. The fundamental disturbances (u_2, v_2, w_2, p_2) take the form of the real

https://doi.org/10.1017/S0022112002003002 Published online by Cambridge University Press

parts of

$$A_0(F_2(r), \mathrm{i}G_2(r), H_2(r), P_2(r))\exp(\mathrm{i}\xi), \qquad \xi = \alpha(x - ct) + N\theta, \tag{2.2}$$

respectively, where α and c are taken to be real and N is an integer. The main aim of the analysis presented in this section is to determine the real amplitude A_0 of the neutral modes and demonstrate its dependence upon the wavenumbers α and N and the basic flow parameters δ and V. In the process the phase shift across the critical layer will be calculated. The wave speed c of the neutral mode is assumed to be $O(1)$ (the precise value will be determined as part of the analysis) and we write $c = c_0$ to leading order.

We substitute the expansions (2.1), (2.2) into the governing equations (1.1) and obtain the leading-order inviscid balances:

$$\alpha F_2 + G_2' + \frac{G_2}{r} + \frac{NH_2}{r} = 0, \qquad (U_0 - c_0)\alpha F_2 + G_2 U_0' = -\alpha P_2, \tag{2.3a, b}$$

$$(U_0 - c_0)\alpha G_2 = P_2', \qquad (U_0 - c_0)\alpha H_2 = -\frac{NP_2}{r}. \tag{2.3c, d}$$

The velocity components F_2, G_2, H_2 can be eliminated, leaving the pressure perturbation governed by Rayleigh's equation:

$$(U_0 - c_0)\left(P_2'' + \frac{1}{r}P_2' - \left(\alpha^2 + \frac{N^2}{r^2}\right)P_2\right) = 2U_0'P_2'. \tag{2.4}$$

The appropriate boundary conditions express the inviscid requirement of tangential flow on the boundaries, namely

$$P_2' = 0 \quad \text{on} \quad r = \delta, \qquad P_2' = 0 \quad \text{on} \quad r = 1. \tag{2.5}$$

As expected it is clear from (2.3) that the velocity components are singular at the radial location where $U_0 = c_0$ and a critical layer is required at this location to smooth out the singularity. We define r_c such that

$$U_0 = c_0 \quad \text{when} \quad r = r_c,$$

and note that for thread–annular flow the critical layer position r_c depends on the values of δ and V.

In what follows we assume that the thread injection velocity V is larger than the (as yet unknown) disturbance wave speed c_0. If this is not the case, and $V < c_0$, then there will be two values of r_c and hence two critical layers to analyse. We will see in § 3 that the condition $V > c_0$ leads to the determination of a critical thread radius below which no instability of the single-critical-layer type is possible. In view of these remarks it is clear that there is a fundamental difference between the stability properties of thread–annular flow with a moving ($V \neq 0$) and non-moving ($V = 0$) thread. It is only the former case that we consider here. The observation here that the stability properties of thread–annular flow depend crucially on whether the thread is moving is consistent with the experiments of FLW where they found major differences between the results for $V = 0$ and $V \neq 0$. We will discuss these experiments in more detail in § 5.

It is convenient at this point to define the skin-friction and curvature coefficients $\tau_0 = -r_c U_0'(r_c)$, $\tau_1 = \frac{1}{2}r_c^2 U_0''(r_c)$. For thread–annular flow these have the explicit form

$$\tau_0 = 2r_c^2 - \frac{V - 1 + \delta^2}{\ln\delta}, \quad \tau_1 = -r_c^2 - \frac{V - 1 + \delta^2}{2\ln\delta},$$

https://doi.org/10.1017/S0022112002003002 Published online by Cambridge University Press

from (1.3). In order to match with the critical layer we need to derive the asymptotic behaviour of the disturbance velocity components and pressure as the critical layer is approached. It is straightforward to show from (2.3) and (2.4) that as $r \to r_c-$

$$F_2 \sim \frac{\hat{p}}{\alpha^2 r_c^2 \tau_0}\left(\frac{N^2}{\varepsilon} + \left(\left(\frac{2\tau_1}{\tau_0} - 1\right)N^2 + \alpha^2 r_c^2\left(1 + \frac{2\tau_1}{\tau_0}\right)\right)\ln\varepsilon \right.$$
$$\left. -3j_3 - \frac{N^2}{3}\left(1 - \frac{2\tau_1}{\tau_0}\right) + \frac{\alpha^2 r_c^2}{3}\left(1 + \frac{5\tau_1}{\tau_0}\right)\right) + O(\varepsilon \ln\varepsilon), \quad (2.6a)$$

$$G_2 \sim -\frac{\hat{p}}{\alpha r_c \tau_0}\left(-(N^2 + \alpha^2 r_c^2) + \left(N^2 - \alpha^2 r_c^2 - \frac{2\tau_1}{\tau_0}(N^2 + \alpha^2 r_c^2)\right)\varepsilon \ln\varepsilon \right.$$
$$+ \left(\tfrac{1}{3}(N^2 - \alpha^2 r_c^2) + 3j_3 + \frac{1}{3}\frac{\tau_1}{\tau_0}(N^2 + \alpha^2 r_c^2)\right)\varepsilon$$
$$\left. + \left(1 + \frac{\tau_1}{\tau_0}\right)\left((N^2 - \alpha^2 r_c^2) - \frac{2\tau_1}{\tau_0}(N^2 + \alpha^2 r_c^2)\right)\varepsilon^2 \ln\varepsilon\right) + O(\varepsilon^2), \quad (2.6b)$$

$$H_2 \sim -\frac{N\hat{p}}{\alpha r_c \tau_0}\left(\frac{1}{\varepsilon} + (1 - \frac{\tau_1}{\tau_0})\right) + O(\varepsilon), \quad (2.6c)$$

$$P_2 \sim \hat{p}\left(1 - \tfrac{1}{2}(N^2 + \alpha^2 r_c^2)\varepsilon^2 + \frac{1}{3}\left(N^2\left(1 - \frac{2\tau_1}{\tau_0}\right) - \alpha^2 r_c^2\left(1 + \frac{2\tau_1}{\tau_0}\right)\right)\varepsilon^3 \ln\varepsilon + j_3\varepsilon^3 \right.$$
$$\left. + \frac{1}{4}\left(1 + \frac{2\tau_1}{\tau_0}\right)\left(N^2\left(1 - \frac{2\tau_1}{\tau_0}\right) - \alpha^2 r_c^2\left(1 + \frac{2\tau_1}{\tau_0}\right)\right)\varepsilon^4 \ln\varepsilon\right) + O(\varepsilon^4), \quad (2.6d)$$

where the small parameter ε is defined by $\varepsilon = (r_c - r)/r_c$, and $\hat{p} = P_2(r_c)$. As in SB and Walton (2002) the quantity j_3 is unknown but can be found numerically by solving the Rayleigh equation (2.4) subject to the boundary conditions (2.5). Finally, there is a jump condition across the critical layer arising from the $O(R^{-1/2})$ phase shift which we determine precisely in the next section. The implication of this is that terms of the form

$$\mathrm{Re}(\ln(r_c - r)\exp(\mathrm{i}\xi)) \quad \text{for} \quad r < r_c$$

are replaced by

$$\mathrm{Re}((\ln(r - r_c) + \mathrm{i}R^{-1/2}\Phi)\exp(\mathrm{i}\xi)) \quad \text{for} \quad r > r_c, \quad (2.7)$$

where the $O(1)$ quantity Φ is to be determined as part of the analysis. This means that quantities such as $\ln(r_c - r)\cos\xi$ are replaced by $\ln(r - r_c)\cos\xi - R^{-1/2}\Phi\sin\xi$ as we cross the critical layer. We therefore see by comparison with the expansions (2.1) that (u_5, v_5, w_5, p_5) will be the lowest-order terms to undergo a non-zero phase shift. As far as the solution of the Rayleigh equation (2.4) is concerned, the appropriate jump condition is simply that P_2 remains real as the critical layer is crossed. As in previous works, the solution of (2.4) subject to the boundary conditions (2.5) and the jump condition will determine the value of the wave speed c_0 for given values of N, α, δ and V. The Rayleigh equation is solved numerically in § 3. Next we investigate the dynamics of the critical layer with the ultimate aim of determining the scaled phase shift Φ analytically in terms of the disturbance amplitude A_0.

https://doi.org/10.1017/S0022112002003002 Published online by Cambridge University Press

2.2. *The inviscid nonlinear critical layer*

The analysis in this section follows closely the work of SB and Walton (2002) and we adopt a similar notation to theirs wherever possible. Rather than presenting all the details here we just present the key results.

First, we can obtain the thickness of the critical layer using the following argument. As the critical layer is approached from the inviscid region we can see that the fundamental azimuthal disturbance $\sim R^{-1/3}\varepsilon^{-1}$, while the pressure $\sim R^{-1/3}$. In the critical layer nonlinear and pressure forces dominate with viscosity a higher-order effect and so we have the balance $p \sim w^2$ from the azimuthal momentum equation (1.1*d*). Thus we have $\varepsilon \sim R^{-1/6}$ in the critical layer and we write

$$r = r_c + R^{-1/6}Y, \quad \text{with} \quad Y = O(1).$$

The velocities and pressure expand as follows:

$$u = c_0 + R^{-1/6}U_1(Y,\xi) + (R^{-1/3}\ln R^{-1/6})U_{3/2}(Y,\xi) + R^{-1/3}U_2(Y,\xi) + \cdots + R^{-5/6}U_5(Y,\xi) + \cdots, \tag{2.8a}$$

$$v = R^{-1/3}V_1(Y,\xi) + (R^{-1/2}\ln R^{-1/6})V_{3/2}(Y,\xi) + R^{-1/2}V_2(Y,\xi) + \cdots + R^{-1}V_5(Y,\xi) + \cdots, \tag{2.8b}$$

$$w = R^{-1/6}W_1(Y,\xi) + (R^{-1/3}\ln R^{-1/6})W_{3/2}(Y,\xi) + R^{-1/3}W_2(Y,\xi) + \cdots + R^{-5/6}W_5(Y,\xi) + \cdots, \tag{2.8c}$$

$$p = R^{-1/3}P_1(Y,\xi) + (R^{-1/2}\ln R^{-1/6})P_{3/2}(Y,\xi) + R^{-1/2}P_2(Y,\xi) + \cdots + R^{-1}P_5(Y,\xi) + \cdots. \tag{2.8d}$$

Substitution of these expansions into the Navier–Stokes equations (1.1) yields the following leading-order nonlinear balances:

$$\alpha U_{1\xi} + V_{1Y} + \frac{NW_{1\xi}}{r_c} = 0, \tag{2.9a}$$

$$\alpha U_1 U_{1\xi} + V_1 U_{1Y} + \frac{NW_1 U_{1\xi}}{r_c} = -\alpha P_1, \quad P_{1Y} = 0, \tag{2.9b,c}$$

$$\alpha U_1 W_{1\xi} + V_1 W_{1Y} + \frac{NW_1 W_{1\xi}}{r_c} = -\frac{NP_{1\xi}}{r_c}, \tag{2.9d}$$

from which we deduce that the main pressure disturbance is constant throughout the layer and assumes the value

$$P_1 = A_0\hat{p}\cos\xi + p_{2M}(r_c),$$

from (2.1), (2.2) and (2.6). In order to match to the inviscid region the appropriate asymptotic behaviour of the velocity components is

$$U_1 \sim -\frac{\tau_0}{r_c}Y + u_{1M}(r_c\pm) - \frac{A_0\hat{p}N^2}{\alpha^2 r_c\tau_0 Y}\cos\xi, \tag{2.10a}$$

$$V_1 \sim -\frac{A_0\hat{p}}{\alpha r_c\tau_0}(N^2+\alpha^2 r_c^2)\sin\xi, \quad W_1 \sim \frac{A_0\hat{p}N}{\alpha\tau_0 Y}\cos\xi + w_{1M}(r_c\pm), \tag{2.10b,c}$$

https://doi.org/10.1017/S0022112002003002 Published online by Cambridge University Press

as $Y \to \pm\infty$, with the first term in (2.10*a*) arising from the basic flow. As in SB this leading-order problem can be solved analytically. It has the form

$$U_1 = -\frac{N}{\alpha r_c} G(\eta), \quad V_1 = -\mu \sin\xi, \quad W_1 = -\frac{\alpha\tau_0}{N}\left(Y - \frac{r_c b}{\tau_0}\right) + G(\eta), \qquad (2.11a\text{–}c)$$

with

$$\mu = \frac{A_0 \hat{p} \Delta}{\alpha r_c \tau_0}, \quad b = u_{1M}(r_c\pm) + \frac{N}{\alpha r_c} w_{1M}(r_c\pm), \quad \Delta = N^2 + \alpha^2 r_c^2. \qquad (2.12)$$

The solution depends on the variable η, a function of Y and ξ given by

$$\eta = \frac{\alpha\tau_0}{2r_c}\left(Y - \frac{r_c b}{\tau_0}\right)^2 + \mu\cos\xi.$$

At this order the function $G(\eta)$ is arbitrary (it will be determined later in (2.25)), but to match to the inviscid region we require the asymptotic behaviour

$$G(\eta) \sim \pm\frac{(2\alpha r_c\tau_0)^{1/2} N}{\Delta}\eta^{1/2} + w_{1M}(r_c\pm) \quad \text{as} \quad \eta \to \infty, \qquad (2.13)$$

implied by (2.10) and (2.11). The $\pm$ signs refer to the upper/lower parts of the critical layer where $Y - r_c b/\tau_0 > (2r_c\mu(1-\cos\xi)/\alpha\tau_0)^{1/2}$, and $Y - r_c b/\tau_0 < -(2r_c\mu(1-\cos\xi)/\alpha\tau_0)^{1/2}$, respectively.

In order to determine the phase shift we need to examine the behaviour of higher-order terms. It is convenient to define a skewed velocity

$$\bar{u}_m = \alpha U_m + \frac{N}{r_c} W_m \qquad (2.14)$$

for $m = 1, 3/2, 2, \ldots$, so that the continuity equation becomes

$$\bar{u}_{m\xi} + V_{mY} = \mathscr{F}_m^{(1)}. \qquad (2.15)$$

Following some manipulation of the governing equations we can obtain an equation for the shear $\bar{u}_{mY}$. This takes the form

$$\mp\left(\frac{2\alpha\tau_0}{r_c}\right)^{1/2}(\eta - \mu\cos\xi)^{1/2}\frac{\partial\bar{u}_{mY}}{\partial\hat{\xi}} = \frac{\partial\mathscr{F}_m^{(2)}}{\partial Y} - \frac{\Delta}{r_c^2}\frac{\partial\mathscr{F}_m^{(3)}}{\partial\xi} + \frac{\alpha\tau_0}{r_c}\mathscr{F}_m^{(1)}. \qquad (2.16)$$

The quantities $\mathscr{F}_m^{(n)}$ ($m = 1, 3/2, 2, \ldots$; $n = 1, 2, 3, 4$) are forcing terms arising from the Navier–Stokes equations which can be written down for any particular m and n, and the transformation of (ξ, Y) to characteristic variables $(\hat{\xi}, \eta)$ with $\xi = \hat{\xi}$ has been performed. A similar equation for W_m can be obtained and takes the form

$$\mp\left(\frac{2\alpha\tau_0}{r_c}\right)^{1/2}(\eta - \mu\cos\xi)^{1/2}\frac{\partial W_m}{\partial\hat{\xi}} = \mu\sin\xi G'(\eta)\bar{u}_m$$
$$+V_m\left(\frac{\alpha\tau_0 N}{\Delta} \mp \left(\frac{2\alpha\tau_0}{r_c}\right)^{1/2}(\eta - \mu\cos\xi)^{1/2}G'(\eta)\right) + \mathscr{F}_m^{(4)} - \frac{N}{r_c}P_{m\xi}. \qquad (2.17)$$

This equation enables W_m to be determined once the shear term $\bar{u}_{mY}$ is found from (2.16). The corresponding equations to (2.16) and (2.17) in SB are their equations (3.10*a*) and (3.10*b*).

In order to induce a phase shift across the critical layer we require the solution for $(\bar{u}_m, W_m, P_m)$ to possess an odd part about $\xi = \pi$, with V_m even. As in SB the $m = 3/2$

https://doi.org/10.1017/S0022112002003002 Published online by Cambridge University Press

solution does not give a phase shift and need not be considered further. Next we consider the $m = 2$ stage for which the forcing terms take the form

$$\mathscr{F}_2^{(1)} = -\frac{V_1}{r_c} + \frac{NY W_{1\xi}}{r_c^2}, \tag{2.18a}$$

$$\mathscr{F}_2^{(2)} = \frac{\alpha N Y W_1 U_{1\xi}}{r_c^2} + \frac{N}{r_c}\left(\frac{NY W_1 W_{1\xi}}{r_c^2} - \frac{V_1 W_1}{r_c} + \frac{NY P_{1\xi}}{r_c^2}\right), \tag{2.18b}$$

$$\mathscr{F}_2^{(3)} = \frac{W_1^2}{r_c}, \quad \mathscr{F}_2^{(4)} = \frac{NY W_1 W_{1\xi}}{r_c^2} - \frac{V_1 W_1}{r_c} + \frac{NY P_{1\xi}}{r_c^2}. \tag{2.18c,d}$$

Here the controlling equations are (2.16), (2.17) with $m = 2$, together with the asymptotic behaviour

$$\begin{aligned} U_2 \sim{}& \frac{\tau_1}{r_c^2} Y^2 + Y u'_{1M}(r_c\pm) + u_{2M}(r_c\pm) \\ &+ \frac{A_0\hat{p}}{\alpha^2\tau_0 r_c^2}\left(\left(-N^2\left(1 - \frac{2\tau_1}{\tau_0}\right) + \alpha^2 r_c^2\left(1 + \frac{2\tau_1}{\tau_0}\right)\right)\ln\left|\frac{Y}{r_c}\right|\right. \\ &\left. - \frac{N^2}{3}\left(1 - \frac{2\tau_1}{\tau_0}\right) - 3j_3 + \frac{\alpha^2 r_c^2}{3}\left(1 + \frac{5\tau_1}{\tau_0}\right)\right)\cos\xi, \end{aligned} \tag{2.19a}$$

$$\begin{aligned} V_2 \sim{}& -\frac{A_0\hat{p}}{\alpha\tau_0 r_c}\left(\left(N^2\left(1 - \frac{2\tau_1}{\tau_0}\right) - \alpha^2 r_c^2\left(1 + \frac{2\tau_1}{\tau_0}\right)\right)\frac{Y}{r_c}\ln\left|\frac{Y}{r_c}\right|\right. \\ &\left. + \left(\frac{1}{3}N^2\left(1 + \frac{\tau_1}{\tau_0}\right) + 3j_3 - \frac{\alpha^2 r_c^2}{3}\left(1 - \frac{\tau_1}{\tau_0}\right)\right)\frac{Y}{r_c}\right)\sin\xi, \end{aligned} \tag{2.19b}$$

$$W_2 \sim Y w'_{1M}(r_c\pm) - \frac{NA_0\hat{p}}{\alpha r_c\tau_0}\left(1 - \frac{\tau_1}{\tau_0}\right)\cos\xi + w_{2M}(r_c\pm), \tag{2.19c}$$

as $Y \to \pm\infty$, implied by (2.6). Integrating the shear equation with respect to $\hat{\xi}$ we obtain

$$\begin{aligned} -\left(\frac{2\alpha\tau_0}{r_c}\right)^{1/2}\bar{u}_{2Y} = {}& \frac{\tau_0^{1/2}}{2^{1/2}r_c}\kappa(\eta) \pm (\eta - \mu\cos\xi)^{1/2}\left(-\frac{2\alpha\tau_0 N^2}{r_c^2\Delta}\right. \\ &\left. + \frac{2\alpha^3\tau_0}{\Delta} - \frac{2N\alpha b}{r_c^2}G' + \frac{4\Delta}{r_c^3}GG'\right) + 2\mu N\left(\frac{2\alpha\tau_0}{r_c^5}\right)^{1/2} G'\cos\xi. \end{aligned} \tag{2.20}$$

From the boundary conditions (2.19) we deduce

$$\bar{u}_{2Y} \sim \frac{2\alpha\tau_1}{r_c^2}Y + \tilde{\lambda}^{\pm} \quad \text{as} \quad Y \to \pm\infty, \tag{2.21}$$

with $\tilde{\lambda}^{\pm} = \alpha u'_{1M}(r_c\pm) + (N/r_c)w'_{1M}(r_c\pm)$ being constants in the upper and lower regions of the critical layer. The difference $\tilde{\lambda}^{+} - \tilde{\lambda}^{-}$ is the vorticity jump across the critical layer, and is crucial both in determining the phase shift and fixing the mean-flow distortions (see § 4). The function $\kappa(\eta)$ in (2.20) is as yet unknown but must satisfy

$$\kappa(\eta) \sim \mp\frac{2^{3/2}\alpha}{r_c\tau_0^{1/2}}(2\tau_1 + \tau_0)\eta^{1/2} \quad \text{as} \quad \eta \to \infty, \tag{2.22}$$

from (2.13), (2.21).

https://doi.org/10.1017/S0022112002003002 Published online by Cambridge University Press

Using 'O' or 'E' to represent contributions that are odd or even about $\xi = \pi$, the forcing terms at the $m = 4$ stage (which include the first effects of viscosity) may be abbreviated to

$$\mathscr{F}_4^{(1)} = \text{`}O\text{'}, \quad \mathscr{F}_4^{(2)} = U_{1YY} + \frac{N}{r_c} W_{1YY} + \text{`}O\text{'}, \tag{2.23a,b}$$

$$\mathscr{F}_4^{(3)} = \text{`}E\text{'}, \quad \mathscr{F}_4^{(4)} = W_{1YY} + \text{`}O\text{'}, \tag{2.23c,d}$$

with the shear governed by

$$\mp \left(\frac{2\alpha\tau_0}{r_c}\right)^{1/2} (\eta - \mu\cos\xi)^{1/2} \frac{\partial \bar{u}_{4Y}}{\partial \hat{\xi}} = \frac{\partial}{\partial Y}\left(U_{1YY} + \frac{N}{r_c} W_{1YY} + \text{`}O\text{'}\right) - \frac{N^2}{r_c^2}\frac{\partial}{\partial \xi}(\text{`}E\text{'}) + \text{`}O\text{'}$$

$$= \bar{u}_{1YYY} + \text{`}O\text{'} = \text{`}O\text{'},$$

since $\bar{u}_{1YYY}$ is zero from (2.11). It follows that $\bar{u}_{4Y}$ is 'E', V_4 is 'O' and P_4 is 'E'. As in SB the equation for W_4 can be integrated with respect to $\hat{\xi}$, leading to

$$\mp W_4 = \left(\frac{2\alpha\tau_0}{r_c}\right)^{1/2} \frac{\partial}{\partial \eta}\left(G'(\eta)\int_0^{\hat{\xi}} (\eta - \mu\cos q)^{1/2}\,\mathrm{d}q\right) + C_4(\eta) + \text{`}E\text{'}, \tag{2.24}$$

with $C_4(\eta)$ an arbitrary function. Imposing the condition of periodicity on W_4 fixes the function $G'(\eta)$ as

$$G'(\eta) = \frac{D^{\pm}}{I(\eta)}, \quad \text{with} \quad I(\eta) = \int_0^{2N\pi} (\eta - \mu\cos q)^{1/2}\,\mathrm{d}q, \qquad D^{\pm} = \pm(2\alpha\tau_0 r_c)^{1/2}\frac{\pi N^2}{\Delta}. \tag{2.25}$$

It follows that

$$G(\eta) \sim G_0 \pm (2\alpha\tau_0 r_c)^{1/2}\frac{N\pi}{\Delta}\left(\frac{\eta^{1/2}}{\pi} + J\right) \quad \text{as} \quad \eta \to \infty, \tag{2.26}$$

with

$$G(\mu) = G_0, \qquad J = \frac{(2\mu)^{1/2}}{8\pi} C^{(1)}, \tag{2.27}$$

where we have uniform vorticity G_0 within the cat's eye and $C^{(1)} \simeq -5.516$ is the same constant as in SB. Hence the finite part of the jump in $G(\eta)$ across the critical layer is determined as

$$[[G(\eta)]]_{-\infty}^{+\infty} = 2(2\alpha\tau_0 r_c)^{1/2}\frac{N\pi}{\Delta} J, \tag{2.28}$$

and this result will be used in the phase shift calculation and the determination of the mean-flow distortions.

The final stage we need to consider (as in SB and Walton 2002) is $m = 5$ where the shear equation is

$$\mp \left(\frac{2\alpha\tau_0}{r_c}\right)^{1/2} (\eta - \mu\cos\xi)^{1/2} \frac{\partial \bar{u}_{5Y}}{\partial \hat{\xi}}$$

$$= \bar{u}_{2YYY} - \frac{N}{r_c^2} V_1 W_{4Y} + \frac{\alpha N \tau_0}{r_c^3} Y W_{4\xi} - \frac{2\Delta}{r_c^3}\frac{\partial}{\partial \xi}(W_1 W_4) + \text{`}O\text{'}. \tag{2.29}$$

By substituting for $\bar{u}_{2Y}$ from (2.20), integrating with respect to $\hat{\xi}$ and demanding

https://doi.org/10.1017/S0022112002003002 Published online by Cambridge University Press

periodicity, we can derive an equation governing the behaviour of the shear term $\kappa(\eta)$. This equation can itself be integrated and after some simplification we obtain

$$\frac{\tau_0 r_c}{4\Delta}(\kappa(\eta)-\kappa_0) = -\frac{\tau_0\alpha^{1/2}N}{r_c^{1/2}\Delta}(\eta G'(\eta) - G(\eta) - \mu G'(\mu) + G_0) - \frac{D_2^{\pm}}{D^{\pm}}(G(\eta)-G_0) - \frac{2\Delta}{\alpha^{1/2}r_c^{3/2}N}\int_{\mu}^{\eta} q(G'(q))^3\,\mathrm{d}q, \quad (2.30)$$

where

$$D_2^{\pm} = \pm(2\tau_0)^{1/2}\frac{\alpha N\pi}{\Delta}\tau_1 \pm \frac{\tau_0^{3/2}\alpha N\pi}{2^{1/2}\Delta}\left(1-\frac{N^2}{\Delta}\right).$$

The finite part of the jump in $\kappa(\eta)$ can then be calculated. We find

$$\frac{\tau_0 r_c}{4\Delta}[[\kappa(\eta)]]_{-\infty}^{+\infty} = \frac{\alpha\pi}{\Delta}(2\tau_0)^{1/2}\left(\frac{3\tau_0 N^2}{\Delta} - (2\tau_1+\tau_0)\right)J + \frac{\alpha\tau_0^{3/2}N^2}{2\Delta^2}\mu^{1/2}\pi - \frac{(2\tau_0)^{3/2}\alpha N^2}{2\Delta^2}(C^{(2)}-2)\mu^{1/2}, \quad (2.31)$$

where

$$C^{(2)} = \frac{8\pi^3N^3}{\mu^{1/2}}\int_{\mu}^{\infty}\left(\frac{s}{I^3} - \frac{1}{8\pi^3N^3s^{1/2}}\right)\mathrm{d}s \simeq 0.1564$$

is a constant which also appears in the analysis of Walton (2002) for impulsively started flow. This term should also be present in SB's analysis of HPF but was overlooked in their work. Using (2.20), (2.31) and the expression (2.27) for J, the vorticity jump across the critical layer can be shown to be

$$\begin{aligned}\tilde{\lambda}^+ - \tilde{\lambda}^- = [[\bar{u}_{2Y}]]_{-\infty}^{+\infty} &= -\frac{1}{2\alpha^{1/2}r_c^{1/2}}[[\kappa(\tilde{\eta})]]_{-\infty}^{+\infty} - \frac{\tau_0^{1/2}\alpha^{1/2}N^2\mu^{1/2}C^{(1)}}{r_c^{3/2}\Delta} \\ &= -\frac{\alpha^{1/2}\tau_0^{1/2}\mu^{1/2}}{r_c^{3/2}}\left(\left(\frac{5N^2}{2\Delta} - \frac{1}{2} - \frac{\tau_1}{\tau_0}\right)C^{(1)} + \frac{N^2}{\Delta}\pi + 2^{3/2}\frac{N^2}{\Delta}(2-C^{(2)})\right).\end{aligned} \quad (2.32)$$

This expression will also prove useful in § 4 when we discuss the mean-flow distortions. In the present context it leads us to an expression for the phase shift. If we write

$$[[\bar{u}_5]]_{-\infty}^{+\infty} = \sum_{n=1}^{\infty}(\beta_n \sin n\xi + \gamma_n \cos n\xi), \quad (2.33)$$

then the phase shift is the coefficient $\beta_1 (= \phi$ say) given by

$$\phi = \frac{1}{N\pi}\int_0^{2N\pi}[[\bar{u}_5]]_{-\infty}^{+\infty}\sin\xi\,\mathrm{d}\xi = \frac{1}{N\pi}\int_{-\infty}^{\infty}\left(\int_0^{2N\pi}\bar{u}_{5Y}\sin\xi\,\mathrm{d}\xi\right)\mathrm{d}Y.$$

The details of the phase shift calculation are given in SB for the special case of HPF and we simply quote the analogous result here, namely

$$\mu\phi = -2(\tilde{\lambda}^+ - \tilde{\lambda}^-) + \frac{4}{r_c^2}\frac{N^2}{\Delta}(2\alpha\tau_0 r_c)^{1/2}\pi J. \quad (2.34)$$

https://doi.org/10.1017/S0022112002003002 Published online by Cambridge University Press

Substituting for $\tilde{\lambda}^+ - \tilde{\lambda}^-$ from (2.32) and J from (2.27) we obtain

$$\mu\phi = \left(\frac{\alpha\tau_0\mu}{r_c^3}\right)^{1/2} \frac{N^2}{\Delta} \left(\left(6 - \frac{\Delta}{N^2}\left(1 + \frac{2\tau_1}{\tau_0}\right)\right) C^{(1)} + 2\pi + 2^{5/2}(2 - C^{(2)}) \right). \quad (2.35)$$

We can now relate ϕ to the scaled phase shift Φ by observing that if the asymptotic form for $\bar{u}_2$ contains a term of the form $k_1 \ln Y \cos\xi$, then in view of the replacement (2.7) we have that $\phi = -k_1\Phi$. From the asymptotic forms (2.6) we see that

$$k_1 = \frac{A_0\hat{p}}{\alpha r_c^2 \tau_0} \left(-N^2 \left(1 - \frac{2\tau_1}{\tau_0}\right) + \alpha^2 r_c^2 \left(1 + \frac{2\tau_1}{\tau_0}\right) \right),$$

and therefore

$$\phi = \frac{A_0\hat{p}}{\alpha r_c^2 \tau_0} \left(N^2 \left(1 - \frac{2\tau_1}{\tau_0}\right) - \alpha^2 r_c^2 \left(1 + \frac{2\tau_1}{\tau_0}\right) \right) \Phi.$$

Finally, we can substitute this relation into (2.35) to determine the phase shift–amplitude relation:

$$\Phi = \frac{r_c(\alpha\tau_0 N)^2}{(A_0\hat{p}\Delta)^{3/2}} \frac{\left(6 - \frac{\Delta}{N^2}\left(1 + \frac{2\tau_1}{\tau_0}\right)\right) C^{(1)} + 2\pi + 2^{5/2}(2 - C^{(2)})}{N^2\left(1 - \frac{2\tau_1}{\tau_0}\right) - \alpha^2 r_c^2 \left(1 + \frac{2\tau_1}{\tau_0}\right)}. \quad (2.36)$$

Confidence in the validity of (2.36) is provided by the fact that it reduces correctly to equation (3.25) of SB for the case of HPF (when $\tau_0 = 2r_c^2$, $\tau_1 = -r_c^2$) with allowance made for the final term involving $C^{(2)}$ which was missed in their analysis. From an examination of the various constants involved it can be seen that the phase shift predicted by (2.36) is always negative. This phase shift should be exactly balanced by that produced by the two wall layers and this will determine the amplitude A_0 of the neutral disturbance. In the next subsection we investigate the dynamics of the wall layers and calculate the phase shift arising from them.

2.3. *The viscous wall layers*

Here we re-introduce the viscous terms neglected to leading order in the critical layer. The dominant balance in both wall layers is between the terms $\alpha(U_0 - c_0)$ and $R^{-1}\partial^2/\partial r^2$, implying a classical $O(R^{-1/2})$ thickness. We deal with the inner wall first, where we write

$$r = \delta + R^{-1/2} r_c Z,$$

where Z is the $O(1)$ normal coordinate within the wall layer. The velocities and pressure expand as

$$u = V + R^{-1/2} U_0'(\delta) r_c Z + \cdots + R^{-1/3}\bar{u}(\xi, Z) + \cdots,$$

$$v = R^{-5/6}\bar{v}(\xi, Z) + \cdots, \qquad w = R^{-1/3}\bar{w}(\xi, Z) + \cdots, \qquad p = R^{-1/3}\bar{p}(\xi, Z) + \cdots,$$

where the scalings here are implied by the behaviour within the inviscid region as $r \to \delta$. The normal momentum equation simplifies to $\partial\bar{p}/\partial Z = 0$ to leading order, implying that the pressure is equal to its value on the thread throughout the layer, i.e. we have

$$\bar{p} = A_0 P_0 \cos\xi + p_{2M}(\delta).$$

https://doi.org/10.1017/S0022112002003002 Published online by Cambridge University Press

The leading-order azimuthal momentum equation takes the form

$$\alpha(V-c_0)\frac{\partial \bar{w}}{\partial \xi} = \frac{NA_0P_0}{\delta}\sin\xi + \frac{1}{r_c^2}\frac{\partial^2 \bar{w}}{\partial Z^2},$$

and the solution of this equation that satisfies no slip on $Z=0$ and remains finite as $Z\to\infty$ is

$$\bar{w} = -\mathrm{Re}\left[\frac{NA_0P_0}{\alpha\delta(V-c_0)}(1-\exp(-mr_cZ))\exp(\mathrm{i}\xi)\right], \qquad m=\left(\frac{1+\mathrm{i}}{\sqrt{2}}\right)\alpha^{1/2}(V-c_0)^{1/2}.$$

Now that the azimuthal velocity is known, the other velocity components can be determined from the continuity and streamwise balances:

$$\alpha\frac{\partial \bar{u}}{\partial \xi} + \frac{1}{r_c}\frac{\partial \bar{v}}{\partial Z} + \frac{N}{\delta}\frac{\partial \bar{w}}{\partial \xi} = 0,$$

$$\alpha(V-c_0)\frac{\partial \bar{u}}{\partial \xi} = \alpha A_0P_0\sin\xi + \frac{1}{r_c^2}\frac{\partial^2 \bar{u}}{\partial Z^2}.$$

The appropriate solutions satisfying the no-slip conditions are

$$\bar{u} = -\mathrm{Re}\left[\frac{A_0P_0}{(V-c_0)}(1-\exp(-mr_cZ))\exp(\mathrm{i}\xi)\right],$$

$$\bar{v} = -\mathrm{Re}\left[\frac{\mathrm{i}A_0P_0}{(V-c_0)\alpha\delta^2}(N^2+\alpha^2\delta^2)\left(\frac{1}{m}-r_cZ-\frac{1}{m}\exp(-mr_cZ)\right)\exp(\mathrm{i}\xi)\right].$$

Taking the limit of the latter expression as $Z\to\infty$ we find

$$v \sim -R^{-5/6}\frac{A_0P_0}{(V-c_0)\alpha\delta^2}(N^2+\alpha^2\delta^2)r_cZ\sin\xi + R^{-5/6}\frac{2(N^2+\alpha^2\delta^2)A_0P_0}{(2\alpha(V-c_0))^{3/2}\delta^2}(\sin\xi-\cos\xi). \tag{2.37}$$

From comparison of (2.37) with (2.1) we see that the first of these terms matches to the term G_2 in the inviscid region while the second displacement term includes the anticipated phase shift and provides the condition on v_5:

$$v_5 \to \frac{2(N^2+\alpha^2\delta^2)A_0P_0}{(2\alpha(V-c_0))^{3/2}\delta^2}(\sin\xi-\cos\xi) \quad \text{as} \quad r\to\delta,$$

where $P_0 = P_2(\delta)$.

A similar analysis can be carried out for the outer wall layer near $r=1$, the only difference being that $U_0\approx 0$ here and so there is no dependence on V. We find that the resulting displacement effect leads to the appropriate condition on v_5 being

$$v_5 \to \frac{2(N^2+\alpha^2)A_0P_1}{(2\alpha c_0)^{3/2}}(\sin\xi+\cos\xi) \quad \text{as} \quad r\to 1 \tag{2.38}$$

(precisely as in SB) where $P_1 = P_2(1)$.

2.4. *The determination of the nonlinear disturbance amplitude by the balancing of phase shifts*

The critical layer analysis of § 2.2 has revealed that the components (u_5, v_5, w_5, p_5) contain terms of the form

$$A_0(F_5(r)\sin\xi, G_5(r)\cos\xi, H_5(r)\sin\xi, P_5(r)\sin\xi)$$

https://doi.org/10.1017/S0022112002003002 Published online by Cambridge University Press

where

$$G_5(\delta) = -\frac{2(N^2+\alpha^2\delta^2)A_0P_0}{(2\alpha(V-c_0))^{3/2}\delta^2}, \qquad G_5(1) = \frac{2(N^2+\alpha^2)A_0P_1}{(2\alpha c_0)^{3/2}}, \tag{2.39}$$

from the wall layer analysis of § 2.3. From substitution into the Navier–Stokes equations we find that P_5 satisfies the same Rayleigh equation as P_2, namely

$$(U_0-c_0)\left(P_5'' + \frac{1}{r}P_5' - \left(\frac{N^2}{r^2}+\alpha^2\right)P_5\right) = 2U_0'P_5',$$

but the boundary conditions are now

$$P_5'(\delta) = -\frac{(N^2+\alpha^2\delta^2)P_0}{(2\alpha(V-c_0))^{1/2}\delta^2}, \qquad P_5'(1) = -\frac{(N^2+\alpha^2)P_1}{(2\alpha c_0)^{1/2}}, \tag{2.40}$$

from (2.39), together with the jump condition

$$[P_5]^+_- = -\left(N^2-\alpha^2r_c^2 - \frac{2\tau_1}{\tau_0}(N^2+\alpha^2r_c^2)\right)\left(\frac{r_c-r}{r_c}\right)^3\frac{\hat{p}}{3}\Phi, \tag{2.41}$$

deduced from the pressure behaviour in (2.6) and the jump (2.7). After some manipulation we obtain

$$\frac{r}{(U_0-c_0)^2}(P_5P_2' - P_2P_5') = \begin{cases} \omega^+, & r > r_c \\ \omega^-, & r < r_c, \end{cases} \tag{2.42}$$

where the constants $\omega^\pm$ are given by

$$\omega^+ = (N^2+\alpha^2)(2\alpha)^{-1/2}c_0^{-5/2}P_1^2, \quad \omega^- = (N^2+\alpha^2\delta^2)(2\alpha)^{-1/2}\delta^{-1}(V-c_0)^{-5/2}P_0^2.$$

Applying the jump condition (2.41) to this expression we find that Φ must be given by

$$\Phi = -\frac{\tau_0^2}{\hat{p}^2(2\alpha)^{1/2}}\left(\frac{(N^2+\alpha^2)P_1^2}{c_0^{5/2}} - \frac{(N^2+\alpha^2\delta^2)P_0^2}{(V-c_0)^{5/2}\delta}\right)\Big/\left(N^2-\alpha^2r_c^2 - \frac{2\tau_1}{\tau_0}(N^2+\alpha^2r_c^2)\right), \tag{2.43}$$

and this represents the overall phase shift across the viscous wall layers. This phase shift must be in tune with that found in (2.36) across the critical layer. Equating our two expressions (2.36) and (2.43) for Φ we obtain the final result

$$A_0 = \frac{2^{1/3}r_c^{2/3}\hat{p}^{1/3}\alpha^{5/3}N^{4/3}}{N^2+\alpha^2r_c^2} \times \left(\frac{\left(6-(N^2+\alpha^2r_c^2)N^{-2}\left(1+2\tau_1/\tau_0\right)\right)(-C^{(1)}) - 2\pi - 2^{5/2}(2-C^{(2)})}{(N^2+\alpha^2)c_0^{-5/2}P_1^2 - (N^2+\alpha^2\delta^2)(V-c_0)^{-5/2}\delta^{-1}P_0^2}\right)^{2/3}, \tag{2.44}$$

where all the quantities on the right-hand side are either known analytically or can be easily computed numerically. It is a straightforward matter to check that this result for the amplitude reduces to the corrected form of SB's equation (3.26) for the special case of HPF.

https://doi.org/10.1017/S0022112002003002 Published online by Cambridge University Press

To determine the wave speed c_0 and the pressure quantities $\hat{p}, P_0$ and P_1 we need to solve the Rayleigh equation (2.4) numerically. This is carried out in the next section and leads to the determination of the amplitude of the neutral modes and their dependence on the thread radius δ and injection velocity V.

3. The numerical solution of the Rayleigh equation

The numerical problem under study here is the solution of

$$(U_0 - c_0)\left(P_2'' + \frac{1}{r}P_2' - \left(\frac{N^2}{r^2} + \alpha^2\right)P_2\right) = 2U_0'P_2' \quad (\delta \leqslant r \leqslant 1), \tag{3.1}$$

where $U_0(r)$ is given by (1.3) and depends on the parameters δ and V. The boundary conditions are

$$P_2'(\delta) = 0, \quad P_2'(1) = 0.$$

In addition we need to apply the condition of zero phase shift at $r = r_c$ where $U_0(r_c) = c_0$. From the asymptotic expansion (2.6) of P_2 as $r \to r_c-$ we can derive the jump in P_2'/P_2. We find that

$$\left[\frac{P_2'}{P_2}\right]_-^+ \sim \frac{1}{r_c}(4j_2|\varepsilon| + 8Kh_1|\varepsilon|^3 \ln|\varepsilon| + 2(4j_4 + Kh_1 - 2j_2^2)|\varepsilon|^3), \tag{3.2}$$

neglecting terms of $O(\varepsilon^5 \ln|\varepsilon|)$, where $\varepsilon = (r_c - r)/r_c$, and j_2, j_4, h_1 and K are coefficients in the series expansion of P_2 and are given explicitly by

$$j_2 = -\tfrac{1}{2}(N^2 + \alpha^2 r_c^2), \qquad j_4 = \overline{j_4} + \frac{3}{4}\left(1 + \frac{2\tau_1}{\tau_0}\right)j_3,$$

$$K = \frac{1}{3}\left((N^2 - \alpha^2 r_c^2) - \frac{2\tau_1}{\tau_0}(N^2 + \alpha^2 r_c^2)\right), \qquad h_1 = \frac{3}{4}\left(1 + \frac{2\tau_1}{\tau_0}\right),$$

$$\overline{j_4} = \frac{1}{48}\left(13N^2 - 6N^4 - \alpha^2 r_c^2 - 12N^2\alpha^2 r_c^2 - 6\alpha^4 r_c^4\right) + \frac{11\alpha^2 r_c^2}{12}\left(\frac{\tau_1}{\tau_0}\right) + (N^2 + \alpha^2 r_c^2)\left(\frac{17}{12}\left(\frac{\tau_1}{\tau_0}\right)^2 - \frac{\tau_2}{\tau_1}\right),$$

with $\tau_2 = -r_c^3 U_0'''(r_c)/6$.

3.1. *The numerical procedure*

Our numerical approach is as follows. First, for given values of axial wavenumber α, azimuthal wavenumber N, thread radius δ and injection velocity V we guess a value for the critical layer location r_c in the range $\delta < r_c < 1$. Then we proceed to solve in $\delta < r < r_c(1 - \varepsilon)$ (with ε suitably small) by marching forward using a Runge–Kutta scheme with initial values $P_2(\delta) = 1$, $P_2'(\delta) = 0$. The value of the unknown constant j_3 can then be found using the ratio $P_2'(r_c(1-\varepsilon))/P_2(r_c(1-\varepsilon))$. Next we solve in $r_c(1 + \varepsilon) < r < 1$ by marching inwards from $r = 1$ where we impose $P_2(1) = 1$, $P_2'(1) = 0$. The jump $[P_2'/P_2]_-^+$ can then be calculated. This whole process is repeated, iterating upon r_c, until (3.2) is satisfied. Once the solution for r_c is obtained, the actual values of $P_2(\delta)$ and $P_2(1)$ can be found, and the wave speed c_0 follows from $U_0(r_c) = c_0$. The amplitude of the neutral mode can then be determined from (2.44). The procedure is repeated for a range of values of α, N, δ and V. It can be

https://doi.org/10.1017/S0022112002003002 Published online by Cambridge University Press

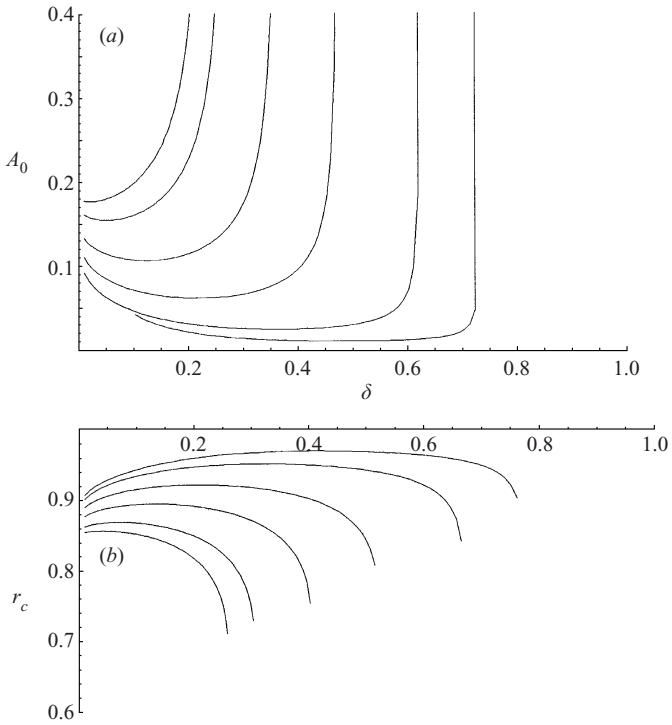


FIGURE 5. Neutral mode results for $N = 1$, $\alpha = 0.01$. (a) Wave amplitude A_0 versus thread radius δ for various injection velocities V. From right to left: $V = 0.1, 0.2, 0.4, 0.6, 0.8, 0.9$. ($b$) Critical layer location r_c versus δ for (from top to bottom) $V = 0.1, 0.2, 0.4, 0.6, 0.8, 0.9$.

demonstrated analytically that the Rayleigh problem posed above has no solution if $N = 0$: we therefore concentrate on non-axisymmetric modes.

3.2. *Numerical results*

In figure 5(a, b) we plot the amplitude of the neutral wave A_0 and the critical layer location r_c versus thread radius δ for various injection velocities V. These results are for a disturbance with axial wavenumber $\alpha = 0.01$ and azimuthal wavenumber $N = 1$. We see that a neutral wave is supported over a range of thread sizes but there is a critical radius (δ_c^+, say) above which no instability exists. This critical radius corresponds to the vanishing of the net phase shift (2.43) across the viscous wall layers: beyond this radius the phase shift is positive and it is no longer possible to balance it against that induced across the critical layer (2.36), which is always negative. It is also evident that this critical radius is generally much less than that which corresponds to the theoretical maximum injection velocity (1.4). We can see from figure 5(a) that δ_c^+ decreases as V increases, while figure 5(b) shows that an increase in injection velocity results in the movement of the critical layer away from the tube wall and towards the thread.

Figure 6(a, b) displays the corresponding results when the axial wavenumber is increased to $\alpha = 0.5$. The general trends described above remain unchanged but the typical amplitude is increased and the instability exists over a slightly smaller range of thread radii. A new feature, evident for $V = 0.1$ (which is shown by a dotted line), is the existence of a lower critical thread radius δ_c^- below which no neutral waves are supported for this value of V. When $\delta < \delta_c^-$, the calculated wave speed c_0 of the

https://doi.org/10.1017/S0022112002003002 Published online by Cambridge University Press

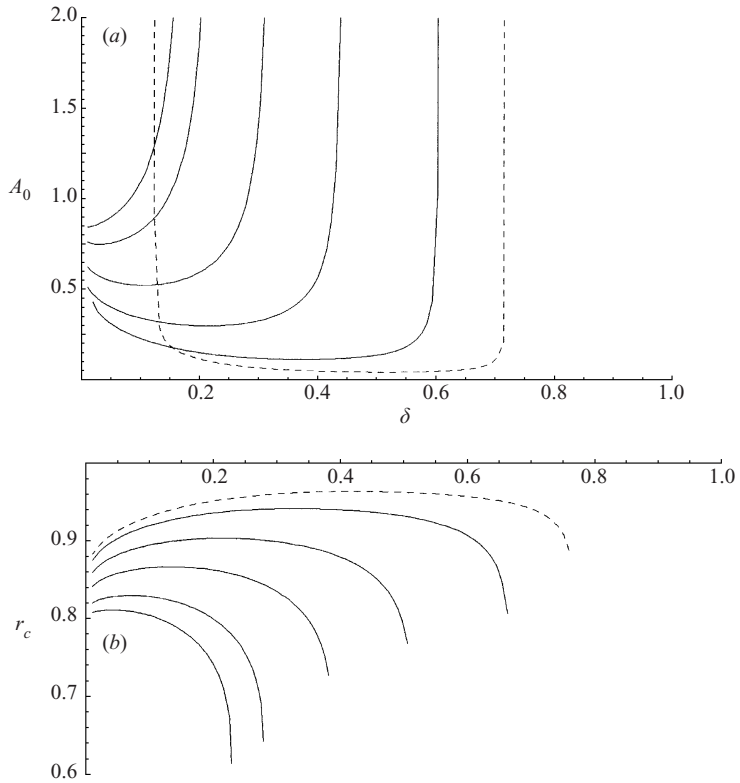


FIGURE 6. Neutral mode results for $N = 1, \alpha = 0.5$. (*a*) Wave amplitude A_0 versus thread radius δ for various injection velocities V. From right to left: $V = 0.1$ (dotted), $0.2, 0.4, 0.6, 0.8, 0.9$. (*b*) Critical layer location r_c versus δ for (from top to bottom) $V = 0.1$ (dotted), $0.2, 0.4, 0.6, 0.8, 0.9$.

disturbance is greater than the injection velocity V. In such a situation (as remarked near the start of § 2) our analysis breaks down since there is no longer a single critical layer in the flow. When α is increased to unity (figure 7) the typical amplitude is raised further, and the lower critical thread radius is evident for both thread velocities $V = 0.1$ and 0.2. The critical layer is sited well away from the wall at this value of axial wavenumber.

Figure 8 shows the results for the situation where the parameters are as in figure 5 except that the azimuthal wavenumber has been increased to $N = 2$. Qualitatively the same dependence of amplitude and critical layer location upon δ is observed with the same trends as V is increased. The typical amplitude, however, is much smaller than in the $N = 1$ case and the range of δ over which an instability of this form exists is reduced, particularly at larger injection velocities. In addition there is a stronger variation of critical layer location with thread radius. These trends continue as N is increased although the ever smaller amplitudes involved make the numerical calculations difficult to perform accurately.

Another approach to the critical phenomena discussed above is to observe that for a given thread radius δ there is a critical injection velocity V_c say, above which the flow is stable to the nonlinear asymmetric disturbances studied here. In figure 9 we plot V_c versus δ. It can be seen that V_c decreases as the axial wavenumber α increases, although V_c is relatively insensitive to changes in α when δ is close to unity. The value of V_c also decreases significantly when the azimuthal wavenumber N is increased

https://doi.org/10.1017/S0022112002003002 Published online by Cambridge University Press

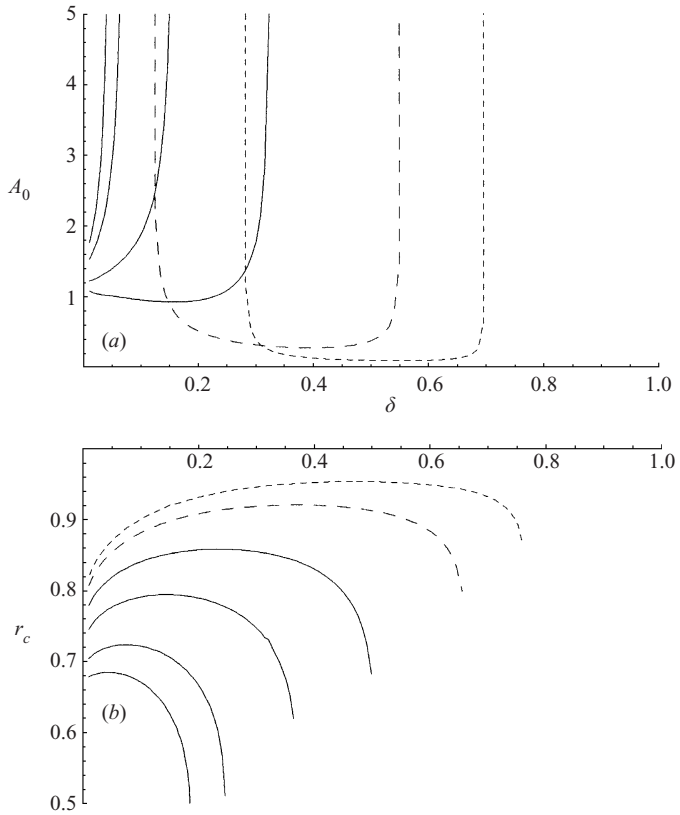


FIGURE 7. Neutral mode results for $N = 1, \alpha = 1$. (*a*) Wave amplitude A_0 versus thread radius δ for various injection velocities V. From right to left: $V = 0.1$ (dotted), 0.2 (dashed), 0.4, 0.6, 0.8, 0.9. (*b*) Critical layer location r_c versus δ for (from top to bottom) $V = 0.1$ (dotted), 0.2 (dashed), 0.4, 0.6, 0.8, 0.9.

from 1 to 2, and this trend continues as N is increased further, suggesting that if the thread velocity is above critical for $N = 1$ the resulting basic flow will also be stable to all higher azimuthal modes. At small values of δ it may be difficult in practice to achieve such stability as figure 9 shows that in such cases the value of V_c is close to or in excess of the maximum achievable thread velocity $V_{\max}$ defined in (1.4). These results therefore suggest that for the thread injection process it is desirable to use a relatively thick thread operating at or above the appropriate value of V_c.

It is interesting to compare our results with the linear stability calculations of Sadeghi & Higgins (1991) where a critical or 'cut-off' velocity, beyond which the flow is linearly stable at all Reynolds numbers, was identified. The thread velocity used in their paper V_{SH} say, can be shown to be related to ours by

$$V = C(\delta)V_{SH}, \qquad C(\delta) = \delta^2 + \frac{1-\delta^2}{2\ln\delta}\left(1 - \ln\left(\frac{\delta^2-1}{2\delta^2\ln\delta}\right)\right).$$

A quick calculation then shows that the cut-off velocities reported in their paper are substantially lower than those found in the nonlinear setting considered here. For example, for the case $\delta = 0.5$, $N = 1$, Sadeghi & Higgins find a cut-off velocity $V_{SH} \simeq 0.6495$, which corresponds to $V_c \simeq 0.082$ using our non-dimensionalization, and is therefore considerably less than the nonlinear cut-off velocity shown in figure 9.

https://doi.org/10.1017/S0022112002003002 Published online by Cambridge University Press

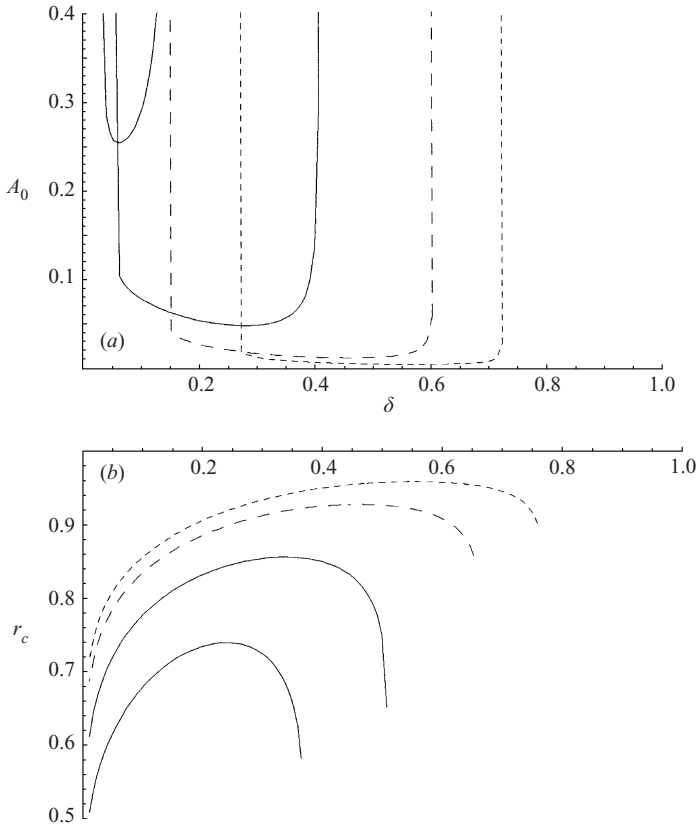


FIGURE 8. Neutral mode results for $N = 2, \alpha = 0.01$. (a) Wave amplitude A_0 versus thread radius δ for various injection velocities V. From right to left: $V = 0.1$ (dotted), 0.2 (dashed), 0.4, 0.6. (b) Critical layer location r_c versus δ for (from top to bottom) $V = 0.1$ (dotted), 0.2 (dashed), 0.4, 0.6.

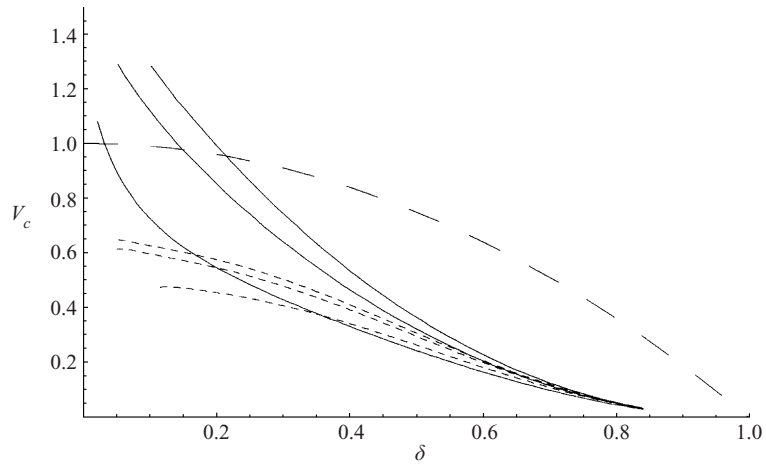


FIGURE 9. Nonlinear cut-off velocity V_c versus δ. The solid curves are for $N = 1$, with (from left to right): $\alpha = 1, 0.5, 0.01$. The dotted lines are for $N = 2$ with (from top to bottom): $\alpha = 0.01, 0.5, 1$. The dashed curve represents the theoretical maximum thread velocity $V_{\max} = 1 - \delta^2$.

https://doi.org/10.1017/S0022112002003002 Published online by Cambridge University Press

This is physically sensible as one would expect a flow operating just above the linear cut-off to still be unstable to finite-amplitude disturbances. Mathematically, as the thread velocity increases, the net phase shift across the viscous wall layers becomes too small to support a linear disturbance, but nonlinear instabilities can still persist.

The fact that nonlinear solutions exist for $N > 1$ is of some interest as the corresponding neutral wave structure for a single pipe only admits the $N = 1$ mode (SB; Walton 2001). Nevertheless, given the typically tiny amplitudes predicted for the higher modes and the associated small cut-off velocities, it would appear that $N = 1$ is likely to dominate in practice and for this reason we will concentrate on the behaviour of this mode in the remainder of the paper.

4. The mean-flow distortions

It can be seen from the expansions (2.1) in the inviscid region that a feature of this instability structure is that the distortion to the mean flow is larger than the fundamental disturbance. Hence when comparing with experiments (as we shall do in § 5) this mean flow distortion is of vital importance and we devote the current section to its determination. From substitution of (2.1) into the Navier–Stokes equations the streamwise mean-flow distortion satisfies

$$u''_{1M} + \frac{1}{r}u'_{1M} = \tfrac{1}{2}A_0^2\left(G_5F'_2 - G_2F'_5 - \frac{NH_5F_2}{r} + \frac{NH_2F_5}{r}\right).$$

Substituting for the quantities on the right-hand side in terms of the pressure, this equation may be rewritten in the form

$$u''_{1M} + \frac{1}{r}u'_{1M} = \tfrac{1}{2}A_0^2\left(\frac{\partial}{\partial r} + \frac{1}{r}\right)\left(\frac{P_5P'_2 - P'_5P_2}{\alpha(U_0 - c_0)^2}\right) = \tfrac{1}{2}A_0^2\left(\frac{\partial}{\partial r} + \frac{1}{r}\right)\left(\frac{\omega^{\pm}}{\alpha r}\right),$$

using the result (2.42) from § 2.4. Since $\omega^{\pm}$ are constants, the right-hand side reduces to zero and therefore the solution for u_{1M} that vanishes on $r = \delta$ and $r = 1$ is simply

$$u_{1M}(r) = \begin{cases} M_1 \ln(r/\delta) & (\delta \leqslant r < r_c) \\ M_2 \ln r & (r_c < r \leqslant 1), \end{cases} \tag{4.1}$$

where M_1 and M_2 are constants to be determined from the jump conditions across the critical layer.

Again, from substitution of (2.1) into the Navier–Stokes equations, the azimuthal mean-flow distortion satisfies

$$\begin{aligned} w''_{1M} + \frac{1}{r}w'_{1M} - \frac{1}{r^2}w_{1M} &= \tfrac{1}{2}A_0^2\left(\alpha H_5F_2 - \alpha F_5H_2 + G_5H'_2 - G_2H'_5 - \frac{H_5G_2}{r} + \frac{G_5H_2}{r}\right) \\ &= \tfrac{1}{2}A_0^2\frac{N}{\alpha^2}\left(\frac{\partial}{\partial r} + \frac{2}{r}\right)\left(\left(\frac{P_5P'_2 - P'_5P_2}{r(U_0 - c_0)^2}\right)\right) \\ &= \tfrac{1}{2}A_0^2\frac{N}{\alpha^2}\left(\frac{\partial}{\partial r} + \frac{2}{r}\right)\left(\frac{\omega^{\pm}}{r^2}\right) \\ &= 0. \end{aligned}$$

Therefore the solution for w_{1M} that vanishes at $r = \delta$ and $r = 1$ is

$$w_{1M}(r) = \begin{cases} M_3(r - \delta^2/r) & (\delta \leqslant r < r_c) \\ M_4(r - 1/r) & (r_c < r \leqslant 1). \end{cases} \tag{4.2}$$

https://doi.org/10.1017/S0022112002003002 Published online by Cambridge University Press

We have four unknown constants $M_1,\ldots,M_4$ and so to fix their values we require four jump conditions across the critical layer. Three of these are easy to obtain from our critical layer calculation. First, from the $m=1$ solution (2.11), (2.12) we have that $\alpha u_{1M}+(N/r_c)w_{1M}$ is continuous, hence

$$[\alpha u_{1M}+(N/r_c)w_{1M}]^{+}_{-}=0. \tag{4.3}$$

Then, from the solution (2.27), (2.28) we have

$$[w_{1M}]^{+}_{-}=[[G(\eta)]]^{+\infty}_{-\infty}=(\alpha\tau_0 r_c\mu)^{1/2}\frac{NC^{(1)}}{2\Delta}\equiv J_1, \tag{4.4}$$

while from (2.19), (2.32) we have

$$\begin{aligned}[\alpha u'_{1M}+(N/r_c)w'_{1M}]^{+}_{-}&=[[\bar{u}_{2Y}]]^{+\infty}_{-\infty}\\ &=-\frac{\alpha^{1/2}\tau_0^{1/2}\mu^{1/2}}{r_c^{3/2}}\left(\left(\frac{5N^2}{2\Delta}-\frac{1}{2}-\frac{\tau_1}{\tau_0}\right)C^{(1)}+\frac{N^2}{\Delta}\pi+2^{3/2}\frac{N^2}{\Delta}(2-C^{(2)})\right)\\ &\equiv J_2,\ \text{say.}\end{aligned} \tag{4.5}$$

To obtain a fourth jump condition further analysis of the critical layer is required, and this is presented in the Appendix. We find that

$$[w'_{1M}]^{+}_{-}=-\frac{(A_0\hat{p})^{1/2}N^3}{r_c\Delta^{3/2}}\left(\left(3-\frac{\Delta}{N^2}\frac{\tau_1}{\tau_0}\right)C^{(1)}+\pi+2^{3/2}(2-C^{(2)})\right)\equiv J_3,\ \text{say.} \tag{4.6}$$

Thus, for given values of V,δ,N and α, the wave amplitude A_0, pressure $\hat{p}$ and critical layer location r_c can be calculated using the numerical method of § 3 and then the quantities J_1,J_2,J_3 can be determined. Applying the jump conditions derived above to the solutions (4.1), (4.2) obtained for the mean-flow distortions we find the constants $M_1,\ldots,M_4$ to take the form

$$M_1=\frac{NJ_3\ln r_c-r_cJ_2\ln r_c-NJ_1/r_c}{\alpha\ln\delta}, \tag{4.7a}$$

$$M_2=\frac{NJ_3\ln(r_c/\delta)-r_cJ_2\ln(r_c/\delta)-NJ_1/r_c}{\alpha\ln\delta}, \tag{4.7b}$$

$$M_3=\frac{(r_c^2-1)}{2(1-\delta^2)}J_3-\frac{(1+r_c^2)}{2r_c(1-\delta^2)}J_1,\qquad M_4=\frac{(r_c^2-\delta^2)}{2(1-\delta^2)}J_3-\frac{(r_c^2+\delta^2)}{2r_c(1-\delta^2)}J_1. \tag{4.7c,d}$$

Figure 10(*a–d*) shows the dependence of the quantities $M_1,\ldots,M_4$ on the thread radius δ as the injection velocity is increased. The wavenumbers of the disturbance in this figure are $\alpha=0.01$ and $N=1$, but qualitatively similar behaviour is found for other choices of α and N. It is clear that the magnitude of the mean-flow quantities (and hence their effect on the basic flow) is generally increased by increasing the injection velocity for a fixed thread radius. Of particular interest here is the quantity M_1 which contributes to the axial shear stress on the thread. In view of the observation that $M_1<0$ for all δ, the effect of the instability is apparently to reduce the force acting on the thread. We investigate this in more detail in the next section.

5. The force on the thread and the friction factor

In the previous two sections we have shown how the basic thread–annular flow is susceptible to a nonlinear instability at high Reynolds number and we have gone

https://doi.org/10.1017/S0022112002003002 Published online by Cambridge University Press

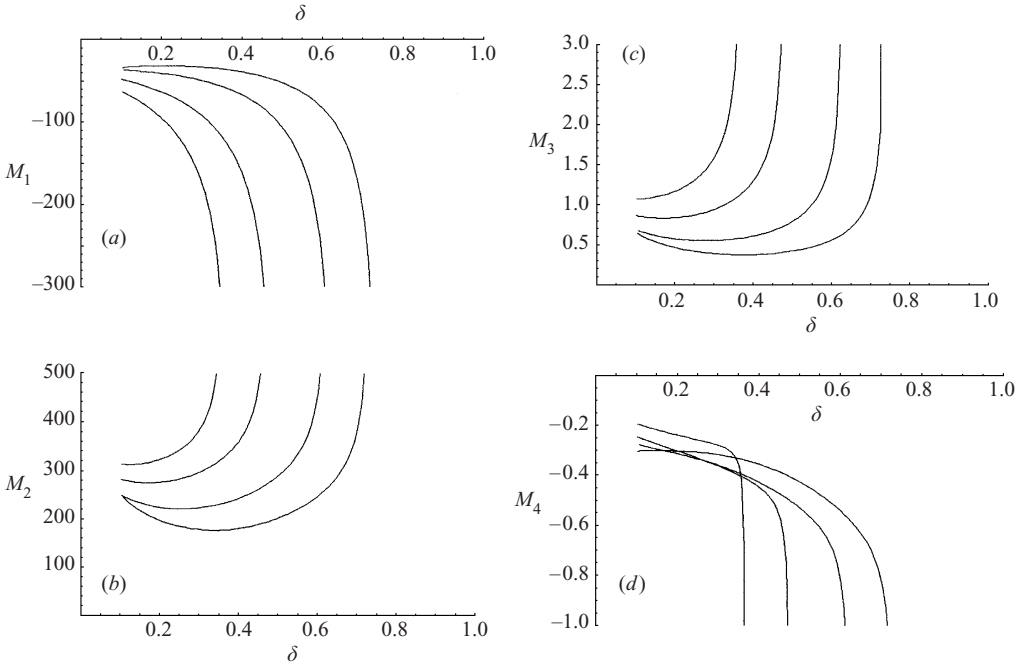


FIGURE 10. Neutral mode results for $N = 1$, $\alpha = 0.01$. The variation of the mean-flow distortion coefficients M_1, M_2, M_3, M_4 with thread radius δ for various injection velocities V. In each plot the values of V are (from right to left) $0.1, 0.2, 0.4, 0.6$.

into some detail in explaining how the amplitude of that disturbance is affected by the size and velocity of the thread. We would like to see whether this instability actually occurs in an experiment and, if so, how it affects quantities that can easily be measured experimentally. In their recent paper, FLW described a thread–annular flow experiment that they performed under controlled conditions. Two of the quantities that they measured were the force on the thread and a quantity known as the 'friction factor' which relates the applied pressure gradient to the flux of fluid through the annular tube. For both quantities they reported a sizeable discrepancy between the experimental measurements and theoretical predictions based on the undisturbed mean-flow profile (1.3). In this section we see what effect the mean flow distortion derived in §4 has on these results and whether it could be responsible for this discrepancy.

It should be noted that in their experiments FLW use a Reynolds number Re which is related to our pressure gradient-based Reynolds number R by

$$Re = \frac{2RQ}{\pi(1+\delta)}, \tag{5.1}$$

where Q is the dimensionless flux of fluid through the annulus (related to the flux $\widehat{Q}$ in FLW by $\widehat{Q} = RQ$) and is given specifically in (5.6) below. The experiments were performed at constant Re rather than constant R. In order to compare with the experimental results for both the resistive force and the friction factor we therefore first compute Q from (5.6) for given R and then calculate the corresponding Re from (5.1). Alternatively, (5.1) and (5.6) together define R implicitly in terms of Re, so that for given values of Re, δ and V, the corresponding R can be calculated numerically.

https://doi.org/10.1017/S0022112002003002 Published online by Cambridge University Press

5.1. *The resistive force on the thread*

Working first in dimensional quantities, the axial shear force on a thread of length l^* is

$$F_\tau^* = 2\pi\delta^* l^* \mu^* \left(\frac{\partial u^*}{\partial r^*}\right)_{r^*=\delta^*}.$$

In terms of the non-dimensional quantities introduced in §1, this becomes

$$F_\tau^* = (\rho^* v^{*2}) 2\pi\delta l R \left(\frac{\partial u}{\partial r}\right)_{r=\delta},$$

where $l^* = a^* l$. Following the notation of FLW we introduce the non-dimensional shear force

$$\widehat{F}_\tau = \frac{F_\tau^*}{\rho^* v^{*2}} = 2\pi\delta l R \left(\frac{\partial u}{\partial r}\right)_{r=\delta}.$$

There is also a pressure force acting on the thread which arises from the constant axial pressure gradient applied to the fluid. This force can be written

$$F_P^* = \pi\delta^{*2} l^* \left(\frac{\partial p^*}{\partial x^*}\right) = (\rho^* v^{*2}) \pi\delta^2 4 l R,$$

and in non-dimensional form as

$$\widehat{F}_P = \frac{F_P^*}{\rho^* v^{*2}} = \pi\delta^2 4 l R.$$

The total resistive force on the thread is therefore

$$\widehat{F}_R = \widehat{F}_\tau + \widehat{F}_P = 2\pi\delta l R \left(\frac{\partial u}{\partial r}\right)_{r=\delta} + \pi\delta^2 4 l R. \tag{5.2}$$

FLW introduce a non-dimensional pressure gradient $\widehat{P} = -(a^{*3}/\rho^* v^{*2})(\partial p^*/\partial x^*)$, which in our notation is equal to $4R$. In their experiments they measure the quantity $\widehat{F}_R/(\widehat{P} l)$ which, from (5.2), can be written

$$\frac{\widehat{F}_R}{\widehat{P} l} = \tfrac{1}{2}\pi\delta \left(\frac{\partial u}{\partial r}\right)_{r=\delta} + \pi\delta^2. \tag{5.3}$$

To calculate $\partial u/\partial r$ we take u equal to $U_0(r) + R^{-1/6} u_{1M}(r)$, with U_0 the basic thread–annular flow given in (1.3) and u_{1M} the mean-flow distortion calculated in (4.1). Substituting for U_0 and u_{1M} we obtain

$$\frac{\widehat{F}_R}{\widehat{P} l} = \frac{\pi}{2}\left(\frac{1-\delta^2}{|\ln\delta|} - \frac{V}{|\ln\delta|} + R^{-1/6} M_1\right), \tag{5.4}$$

where the constant M_1 is given in (4.7). The expression (5.4) is analogous to equation (20) of FLW with the inclusion of the mean-flow distortion arising from the instability. Note that the thread injection velocity V is equal to $4\hat{w}_{TH}/\widehat{P}$ in FLW's notation. In theory it is possible for the total thread force to be zero. In the absence of an instability this occurs when the thread velocity is given by

$$V_{\max} = 1 - \delta^2,$$

as this makes the right-hand side of (5.4) zero. This is said to be the maximum theoretically achievable thread velocity for thread injection.

https://doi.org/10.1017/S0022112002003002 Published online by Cambridge University Press

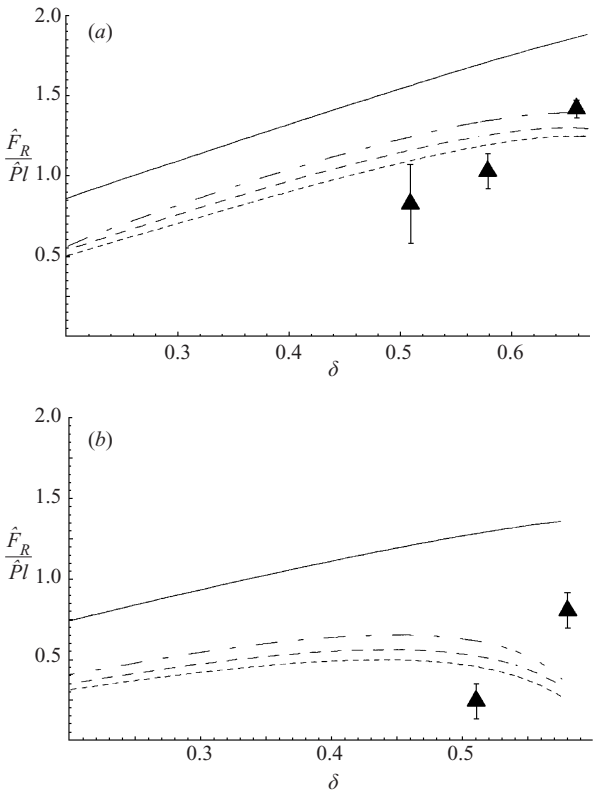


FIGURE 11. Normalized axial thread force versus thread radius δ. (*a*) $N = 1$, $V = 0.08$, $Re = 100$. Results incorporating mean-flow distortion due to instability with $\alpha = 0.01$ (dotted), 0.1 (dashed), 0.5 (dot-dashed). (*b*) $N = 1$, $V = 0.2$, $Re = 100$ with $\alpha = 0.01$ (dotted), 0.1 (dashed), 0.5 (dot-dashed). On both plots the solid curve is the undisturbed theoretical result and the triangles are the experimental measurements of FLW.

In figure 11(*a*, *b*) we plot the resistive force calculated from (5.4) as a function of thread radius δ for two different injection velocities $V = 0.08$ and $V = 0.2$, corresponding to those used in the experiments of FLW, with $Re = 100$. This figure should be compared with figure 5 in FLW. On figure 11 we also include the undisturbed results (i.e. those obtained by setting $M_1 = 0$) and FLW's experimental results. A feature of the results (anticipated at the end of the previous section) is that the thread force for given δ and V is reduced by the presence of the instability. It can be seen that the results are relatively insensitive to changes in the axial wavenumber α. Only the $N = 1$ instability mode is presented here for reasons given towards the end of §3. The predicted thread forces agree quite well with the limited data available from the experiments of FLW who noted the discrepancy with the undisturbed flow theory in their paper. This discrepancy increases with increasing thread velocity and this observation is consistent with our theory. We should mention here that FLW also carried out experiments at zero thread velocity for which our theory is not valid and they also measured the force at thread radii in excess of δ_c^+, which again is not covered by the present theory. Nevertheless the broad agreement between theory and experiment is encouraging and offers a possible reason for the theoretical–experimental discrepancy reported by FLW. It should be noted that although the flux-based Reynolds number Re is only 100 for these experiments, the corresponding values of R (deduced

https://doi.org/10.1017/S0022112002003002 Published online by Cambridge University Press

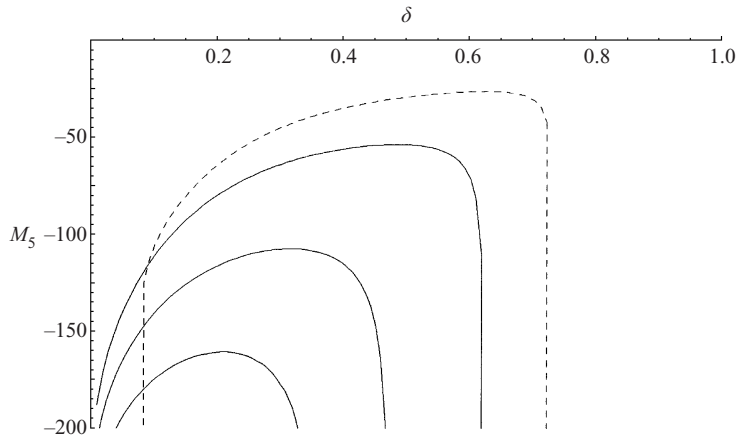


FIGURE 12. Neutral mode results for $N = 1, \alpha = 0.01$. The flux distortion coefficient M_5 versus δ for (from top to bottom): $V = 0.1$ (dotted), $0.2, 0.4, 0.6$.

from (5.1), (5.6)) were as large as 50 000 in some cases, emphasizing the validity of a high-Reynolds-number approach.

5.2. *The friction factor*

In their paper FLW also measure a dimensionless quantity known as the friction factor λ which is essentially the ratio of the pressure gradient along the tube to the square of the mean flow through it. More precisely, λ is given by

$$\lambda = -\frac{16\pi^2}{RQ^2}(1-\delta)(1-\delta^2)^2, \tag{5.5}$$

where Q is the dimensionless flux of fluid through the tube. The expression (5.5) is equivalent to equation (24) in FLW. Taking the flow to be the basic thread–annular solution plus the leading-order axial mean-flow distortion induced by the disturbance, as in § 5.1, we have

$$\begin{aligned} Q &= 2\pi \int_\delta^1 (U_0(r) + R^{-1/6} u_{1M}(r))\, r \,\mathrm{d}r \\ &= \frac{\pi}{2}\left(1 - \delta^4 + \frac{(1-\delta^2)^2}{\ln\delta} - \left(2\delta^2 + \frac{(1-\delta^2)}{\ln\delta}\right) V + R^{-1/6} M_5\right), \end{aligned} \tag{5.6}$$

where

$$M_5 = 4\int_\delta^1 u_{1M}(r)\, r \,\mathrm{d}r = M_1\left(2r_c^2 \ln(r_c/\delta) + \delta^2 - r_c^2\right) + M_2(r_c^2 - 1 - 2r_c^2 \ln r_c).$$

Here we have substituted for u_{1M} from (4.1), while M_1, M_2 are given in (4.7). Thus λ can be calculated from (5.5) with Q given in (5.6). The flux distortion M_5 is plotted versus δ in figure 12 for various values of V, with $\alpha = 0.01$ and $N = 1$. We see that since this quantity appears to always be negative, it has the effect of reducing the overall flux compared to the undisturbed case, with the effect becoming stronger as the injection velocity is increased.

We compare with FLW's experimental results in figure 13 where we plot $\log_{10}|\lambda|$ versus $\log_{10} Re$, where Re is the flux-based Reynolds number used by FLW and is defined above in (5.1). This plot should be compared with FLW's figure 7. We present

https://doi.org/10.1017/S0022112002003002 Published online by Cambridge University Press

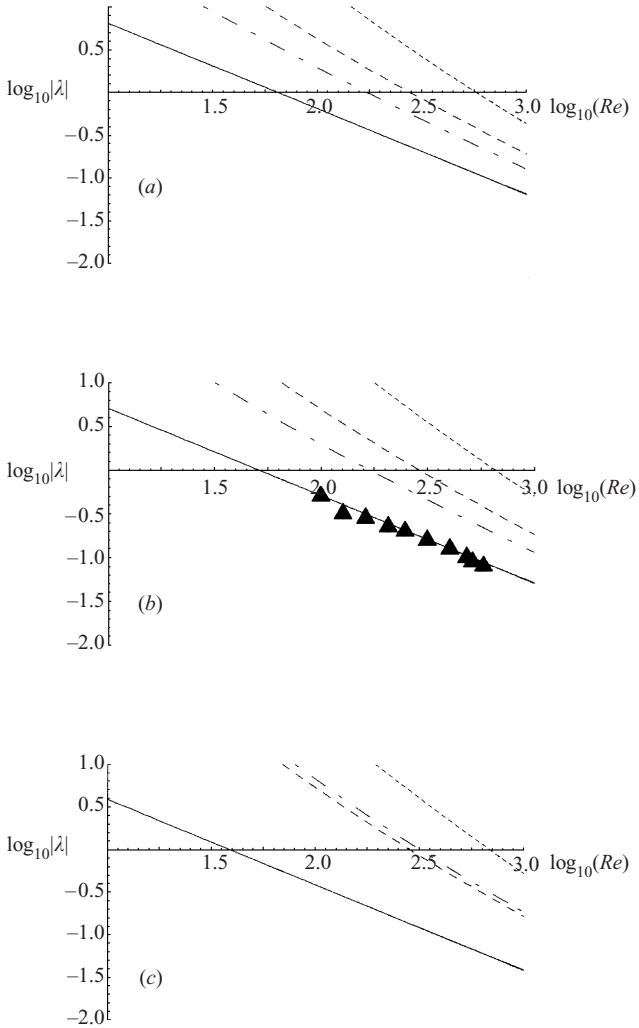


FIGURE 13. Log–log plots of friction factor λ versus flux Reynolds number Re. In each plot results incorporating the mean-flow distortion are shown with $\alpha = 0.01$ (dotted), 0.1 (dashed), 0.5 (dot-dashed). The solid lines are the undisturbed theoretical results and the triangles represent the experimental data of FLW. (*a*) $V = 0.1$; (*b*) $V = 0.178$ (corresponding to an experiment of FLW); (*c*) $V = 0.3$. All the results are for a thread radius $\delta = 0.51$.

plots for thread radius $\delta = 0.51$ and at three different thread velocities with the second of these ($V = 0.178$) corresponding to one of FLW's experiments. The corresponding undisturbed friction factor (which is proportional to $1/Re$) is also plotted in these figures. Once again the azimuthal wavenumber of the disturbance is taken to be $N = 1$ and we show curves for different values of α $(0.01, 0.1, 0.5)$. We can see that in all cases the effect of the instability is to increase the friction factor, essentially by reducing the mass flux Q due to the negative contribution from the term M_5. In contrast FLW measured λ to be slightly less than the undisturbed value and observed an increased flux. They attributed this to radial movement of the thread which in reality is elastic and whose shape will be affected by any non-axial velocity components present in the flow. Our model assumes the thread to be rigid and clearly the incorporation of

https://doi.org/10.1017/S0022112002003002 Published online by Cambridge University Press

thread flexibility would be a useful extension which will be considered in future work on this subject. In addition the upper limit on R for the friction factor experiment turns out to only be about 1000, and we would therefore not necessarily expect our asymptotic theory to perform well in this case.

6. Discussion and future work

In this paper we have modelled the surgical procedure of thread injection by considering the incompressible axial flow between concentric cylinders where the inner cylinder, representing the thread, moves in the axial direction at a constant speed. For this flow we have derived the corresponding exact solution of the Navier–Stokes equations. This model has been used by previous workers in the field, notably Koch & Feind (1958); Shigechi & Lee (1991) and FLW. Motivated by the discrepancy between the undisturbed theory and experiment reported in the last of these references we considered the nonlinear stability of this flow at high Reynolds number. The instability structure is such that a single non-axisymmetric mode dominates across most of the annulus, but within the critical layer (where the disturbance phase speed equals the basic flow velocity) the flow is fully three-dimensional. The critical layer is of the equilibrium, inviscid, nonlinear type previously studied by Benney & Bergeron (1969), Haberman (1972) and SB and produces a small amplitude-dependent phase shift. By balancing this against the net phase shift across the viscous wall layers the amplitude of the neutral modes can be calculated analytically as a function of the axial (α) and azimuthal (N) wavenumbers, the thread radius δ and the injection velocity V. In § 3 we presented results for certain values of these parameters and showed that neutral modes exist over a wide range of thread radii and injection velocities. It is found that although there are no axisymmetric instabilities, solutions for $N > 1$ exist, in contrast to the single pipe case where $N = 1$ is the only instability mode possible. For a given thread radius the amplitude of the neutral mode increases as V increases, but if the injection velocity is sufficiently large the aforementioned balance of phase shifts does not prove possible and the instability ceases to exist in its present form. This 'cut-off' velocity is analogous to that found in linear theory, but is considerably larger in magnitude. Conversely, for a given injection velocity there is an upper thread radius beyond which this instability does not operate, and for small thread velocities there is also a lower limit on the radius.

In terms of the medical application the results of our analysis suggest that it is desirable to use a relatively thick thread operated at as high an injection velocity as possible in order to minimize the lateral movements of the thread during the injection process. This is in contrast to linear theory which predicts that very thin threads are the most stable, irrespective of the injection velocity. Above the nonlinear cut-off velocity V_c the stability properties of the flow are open to conjecture. By analogy with the linear cut-off analysis for Poiseuille–Couette flow (Cowley & Smith 1985) we would expect that rather than the flow being completely stable above V_c, there is a bifurcation to a larger-amplitude unstable state.

The nonlinear disturbance considered in this paper induces a relatively large mean-flow distortion and this is derived explicitly in § 4 and used in § 5 to predict the axial thread force. It is found that the effect of the instability is to reduce the thread force significantly and our results are in line with the experiments performed by FLW. We also derive the disturbed friction factor – this is found to be larger than the undisturbed case due to a reduction in the flux. This was not observed by FLW, whose experiments agreed well with undisturbed-flow theory for non-zero thread

https://doi.org/10.1017/S0022112002003002 Published online by Cambridge University Press

velocities. There are a number of possible reasons for this disagreement and among the most likely are that the Reynolds number in the friction factor experiments was not sufficiently large for our asymptotic theory to be valid, and that the thread assumed an eccentric position within the tube. The experiments reported in FLW were carried out for only a few choices of δ and V, and it would be desirable to compare with experiment over a larger region of parameter space.

The theory presented here could be extended in many ways. More analysis of the disturbance behaviour close to the cut-off in δ or V would be of interest, as would analysis of the $V = 0$ case where two critical layers are present. This latter problem is of considerable interest as the experiments of FLW showed there to be a marked difference in the flow behaviour when the thread is kept fixed. In addition there are a number of refinements that would make the model more realistic. For example the flexibility and eccentricity of the thread (treated here as a concentric rigid body) should be taken into account, while the basic flow could be regarded as still evolving temporally (as in Walton 2002) after the application of the pressure gradient, or spatial evolution could be considered (particularly relevant near the leading edge of the thread).

Nevertheless, we believe that by demonstrating that nonlinear neutral waves can be supported by the basic thread–annular flow we have made a first step towards understanding the stability properties of the thread injection process and have gone some way towards explaining the reported discrepancy between theory and experiment.

The comments of the referees are gratefully acknowledged.

Appendix. Calculation of the jump in w'_{1M} across the critical layer

To calculate this quantity we need to consider the velocity components at the $m = 5$ level, for which the forcing terms of relevance here are

$$\mathscr{F}_5^{(1)} = \frac{NY}{r_c^2} W_{4\xi} + \text{`}O\text{'}, \tag{A 1a}$$

$$\mathscr{F}_5^{(4)} = W_{2YY} + \frac{W_{1Y}}{r_c} - \alpha(U_2 W_{4\xi} + U_4 W_{2\xi}) - V_2 W_{4Y} + \frac{V_1 W_4}{r_c} - \frac{N}{r_c}\frac{\partial}{\partial \xi}(W_2 W_4) - \frac{NY}{r_c^2}\frac{\partial}{\partial \xi}(W_1 W_4) + \text{`}O\text{'}. \tag{A 1b}$$

The azimuthal momentum equation (2.17) has the form

$$\mp\left(\frac{2\alpha\tau_0}{r_c}\right)^{1/2}(\eta - \mu\cos\xi)^{1/2}\frac{\partial W_5}{\partial \hat{\xi}} = \mathscr{F}_5^{(4)} - \frac{N}{r_c}P_{5\xi} - V_5 W_{1Y} - \bar{u}_5 W_{1\xi}.$$

Integrating this equation across the critical layer and using the periodicity of W_5 we have

$$\int_0^{2\pi}\int_{-\infty}^{+\infty}\left(\mathscr{F}_5^{(4)} - \frac{N}{r_c}P_{5\xi} - V_5 W_{1Y} - \bar{u}_5 W_{1\xi}\right) \mathrm{d}Y\, \mathrm{d}\xi = 0.$$

The term involving P_5 integrates to zero upon applying the condition of periodicity. Then, integrating by parts with respect to ξ and using continuity, this equation simplifies to

$$\int_0^{2\pi}\int_{-\infty}^{+\infty}(\mathscr{F}_5^{(4)} + \mathscr{F}_5^{(1)} W_1)\, \mathrm{d}Y\, \mathrm{d}\xi - \int_0^{2\pi}[V_5 W_1]_{-\infty}^{+\infty}\, \mathrm{d}\xi = 0.$$

https://doi.org/10.1017/S0022112002003002 Published online by Cambridge University Press

Using (A 1) for $\mathscr{F}_5^{(1)}$ and $\mathscr{F}_5^{(4)}$ and recognizing that there is no contribution from the 'O' parts, the first integral can be written as

$$I_1 = \int_0^{2\pi}\int_{-\infty}^{+\infty} \left(W_{2YY} + \frac{W_{1Y}}{r_c} - \alpha(U_2 W_{4\xi} + U_4 W_{2\xi}) \right.$$
$$\left. - V_2 W_{4Y} + \frac{V_1 W_4}{r_c} + \frac{NY W_{4\xi} W_1}{r_c^2} \right) \mathrm{d}Y\, \mathrm{d}\xi.$$

Consider the contribution

$$I_{11} = \int_0^{2\pi}\int_{-\infty}^{+\infty} -\alpha(U_2 W_{4\xi} + U_4 W_{2\xi}) - V_2 W_{4Y} + \frac{V_1 W_4}{r_c} + \frac{NY W_{4\xi} W_1}{r_c^2}\, \mathrm{d}Y\, \mathrm{d}\xi.$$

We know from the critical layer calculations that $\bar{u}_4 = \alpha U_4 + (N/r_c)W_4$ is even: this means that we can replace αU_4 by $-(N/r_c)W_4$ in the above expression. Thus,

$$I_{11} = \int_0^{2\pi}\int_{-\infty}^{+\infty} \left(-\alpha U_2 W_{4\xi} + \frac{N}{r_c} W_4 W_{2\xi} - V_2 W_{4Y} + \frac{V_1 W_4}{r_c} + \frac{NY W_{4\xi} W_1}{r_c^2} \right) \mathrm{d}Y\, \mathrm{d}\xi$$
$$= \int_0^{2\pi}\int_{-\infty}^{+\infty} \left(-\alpha U_2 W_{4\xi} + W_4(\mathscr{F}_2^{(1)} - V_{2Y} - \alpha U_{2\xi}) \right.$$
$$\left. - V_2 W_{4Y} + \frac{V_1 W_4}{r_c} + \frac{NY W_{4\xi} W_1}{r_c^2} \right) \mathrm{d}Y\, \mathrm{d}\xi,$$

using the continuity equation (2.15) with $m = 2$. Substituting for $\mathscr{F}_2^{(1)}$ from (2.18) we obtain

$$I_{11} = \int_0^{2\pi}\int_{-\infty}^{+\infty} \left(-\alpha \frac{\partial}{\partial \xi}(U_2 W_4) + \frac{NY}{r_c^2}\frac{\partial}{\partial \xi}(W_4 W_1) - \frac{\partial}{\partial Y}(V_2 W_4) \right) \mathrm{d}Y\, \mathrm{d}\xi$$
$$= -\int_0^{2\pi} [V_2 W_4]_{-\infty}^{+\infty}\, \mathrm{d}\xi,$$

where the first two terms have integrated to zero due to periodicity. The remaining contribution to I_1 is

$$I_{12} = \int_0^{2\pi}\int_{-\infty}^{+\infty} \left(W_{2YY} + \frac{W_{1Y}}{r_c} \right) \mathrm{d}Y\, \mathrm{d}\xi$$
$$= 2\pi \left([w'_{1M}(r_c)]_-^+ + \frac{1}{r_c}[w_{1M}(r_c)]_-^+ \right),$$

from (2.10) and (2.19). So we have that

$$2\pi \left([w'_{1M}(r_c)]_-^+ + \frac{1}{r_c}[w_{1M}(r_c)_-^+] \right) - \int_0^{2\pi} [V_2 W_4]_{-\infty}^{+\infty}\, \mathrm{d}\xi - \int_0^{2\pi} [V_5 W_1]_{-\infty}^{+\infty}\, \mathrm{d}\xi = 0. \quad \text{(A 2)}$$

Note that since V_2 is odd, the component W_4 must also have an odd part to give a contribution. However it can be seen from an inspection of (2.24) that the 'O' part of $W_4 \to 0$ as $Y \to \pm\infty$ and therefore the term $V_2 W_4$ will give no contribution.

We now need to consider the term involving V_5. Since W_1 is even we need information about the even part of V_5. From (2.33) we see that the jump in the odd part of $\bar{u}_5$ is $\phi \sin \xi$ and hence by continuity the jump in the even part of V_5 is

https://doi.org/10.1017/S0022112002003002 Published online by Cambridge University Press

$-\phi Y\cos\xi$. Using the asymptotic form (2.10) for W_1 we conclude that

$$\int_0^{2\pi}[V_5W_1]_{-\infty}^{+\infty}\,\mathrm{d}\xi=-\phi\frac{A_0N\hat{p}}{\alpha\tau_0}\int_0^{2\pi}\cos^2\xi\,\mathrm{d}\xi=-\pi\phi\frac{A_0N\hat{p}}{\alpha\tau_0}.$$

We also have that

$$[w_{1M}(r_c)]_-^+=[[G]]_{-\infty}^{+\infty}=2(2\alpha\tau_0r_c)^{1/2}\frac{N\pi}{\Delta}J,$$

from (2.28). Putting this information together, (A 2) reduces to

$$2\pi[w'_{1M}(r_c)]_-^+ +4\left(\frac{2\alpha\tau_0}{r_c}\right)^{1/2}\frac{N\pi^2}{\Delta}J+\pi\phi\frac{A_0N\hat{p}}{\alpha\tau_0}=0.$$

Substituting for ϕ from (2.35), μ from (2.12) and J from (2.27), we finally obtain the result

$$[w'_{1M}(r_c)]_-^+=-\frac{(A_0\hat{p})^{1/2}N^3}{r_c\Delta^{3/2}}\left(\left(3-\frac{\Delta}{N^2}\frac{\tau_1}{\tau_0}\right)C^{(1)}+\pi+2^{3/2}(2-C^{(2)})\right).$$

This is the expression (referred to as J_3) used to help determine the arbitrary constants in the mean-flow distortions of § 4.

REFERENCES

Benney, D. J. & Bergeron, R. F. 1969 A new class of nonlinear waves in parallel flows. *Stud. Appl. Maths* **48**, 181–204.

Chen, J. N. & Lin, S. P. 2002 Instability of an annular jet surrounded by a viscous gas in a pipe. *J. Fluid Mech.* **450**, 235–258.

Cowley, S. J. & Smith, F. T. 1985 On the stability of Poiseuille–Couette flow: a bifurcation from infinity. *J. Fluid Mech.* **156**, 83–100.

Frei, Ch., Lüscher, P. & Wintermantel, E. 2000 Thread–annular flow in vertical pipes. *J. Fluid Mech.* **410**, 185–210 (referred to herein as FLW).

Haberman, R. 1972 Critical layers in parallel flows. *Stud. Appl. Maths* **51**, 139–161.

Huang, A. & Joseph, D. D. 1995 Stability of eccentric core-annular flow. *J. Fluid Mech.* **282**, 233–245.

Koch, R. & Feind, K. 1958 Druckverlust und Wärmeübergang in Ringspalten. *Chemie Ing. Techn.* **9**, 577–584.

Mott, J. E. & Joseph, D. D. 1968 Stability of parallel flow between concentric cylinders. *Phys. Fluids* **11**, 2065–2073.

Preziosi, L., Chen, K. & Joseph, D. D. 1989 Lubricated pipelining: stability of core-annular flow. *J. Fluid Mech.* **201**, 323–356.

Sadeghi, V. M. & Higgins, B. G. 1991 Stability of sliding Couette–Poiseuille flow in an annulus subject to axisymmetric and asymmetric disturbances. *Phys. Fluids* A **3**, 2092–2104.

Shen, J. & Li, X. 1996 Instability of an annular viscous liquid jet. *Acta Mech.* **114**, 167–183.

Shigechi, T. & Lee, Y. 1991 An analysis on fully developed laminar fluid flow and heat transfer in concentric annuli with moving cores. *Intl J. Heat Mass Transfer* **34**, 2593–2601.

Smith, F. T. & Bodonyi, R. J. 1982 Amplitude-dependent neutral modes in the Hagen–Poiseuille flow through a circular pipe. *Proc. R. Soc. Lond.* A **384**, 463–489 (referred to herein as SB).

Walton, A. G. 2001 The existence of neutral Rayleigh waves in the Hagen–Poiseuille flow through a pipe of circular cross-section. *Stud. Appl. Maths* **106**, 315–335.

Walton, A. G. 2002 The temporal evolution of neutral modes in the impulsively started flow through a circular pipe and their connection to the nonlinear stability of Hagen–Poiseuille flow. *J. Fluid Mech.* **457**, 339–376.

https://doi.org/10.1017/S0022112002003002 Published online by Cambridge University Press